AEDC-TR-69-229

NON-EQUILIBRIUM FLOW FIELDS WITH CHEMICAL REACTIONS IN A SHOCK TUBE

Elihu Zimet and Peter P. Wegener
Department of Engineering and Applied Science
Yale University

October 1969

ARNOLD ENGINEERING DEVELOPMENT CENTER
AIR FORCE SYSTEMS COMMAND
ARNOLD AIR FORCE STATION, TENNESSEE

NOTICES

When U. S. Government drawings specifications, or other data are used for any purpose other than a definitely related Government procurement operation, the Government thereby incurs no responsibility nor any obligation whatsoever, and the fact that the Government may have formulated, furnished, or in any way supplied the said drawings, specifications, or other data, is not to be regarded by implication or otherwise, or in any manner licensing the holder or any other person or corporation, or conveying any rights or permission to manufacture, use, or sell any patented invention that may in any way be related thereto.

Qualified users may obtain copies of this report from the Defense Documentation Center.

References to named commercial products in this report are not to be considered in any sense as an endorsement of the product by the United States Air Force or the Government.

NON-EQUILIBRIUM FLOW FIELDS WITH CHEMICAL REACTIONS IN A SHOCK TUBE

Elihu Zimet and Peter P. Wegener
Department of Engineering and Applied Science
Yale University

FOREWORD

The work reported herein was sponsored by Arnold Engineering Development Center (AEDC), Air Force Systems Command (AFSC), Arnold Air Force Station, Tennessee. Technical monitoring of the contract was performed by Captain Carlos Tirres, USAF, Research Division, Directorate of Plans and Technology.

The effort was conducted from June 1967 to June 1969, at Yale University, under Contract AF 40(600)-1133, Air Force Program Element 62201F, Project 8952, Task 08.

The present technical report is the second under this contract and it was submitted for publication on 22 July 1969.

The reproducibles used for the reproduction of this report were supplied by the authors.

This technical report has been reviewed and is approved.

Carlos Tirres
Captain, USAF
Research Division
Directorate of Plans
and Technology

Harry L. Maynard
Colonel, USAF
Director of Plans
and Technology

ABSTRACT

The present work is concerned with a theoretical and an experimental treatment of non-equilibrium flow of a chemically reacting gas mixture through a shock wave. The two chemical reactions given by $N_2O_4 + M = 2NO_2 + M = 2NO + O_2 + M$, where M represents the inert carrier gases argon or nitrogen, were studied. The experiments were carried out in a temperature controlled shock tube and a light absorption technique permitted the time dependent concentration of the species NO_2 to be determined. For shock strengths where the temperature did not exceed 400°K only the first chemical reaction took place. Stronger shock waves excited both chemical reactions with temperatures up to 2100°K, and for this reason, flow fields with two non-equilibrium modes could be investigated. Since the relaxation times of these two reactions were different by about three orders of magnitude, they could be experimentally uncoupled. A study of the reaction mechanisms and rate constants for both reactions was carried out. In general, the experimental work agreed well with an analytical description of the non-equilibrium flow fields, and with the work of previous investigators at conditions where direct comparisons could be made. At shock strengths exciting only the first chemical reaction the complete picture of a non-equilibrium flow field with only one non-equilibrium mode could be investigated. In this situation, the shock strengths were varied from weak, fully dispersed waves to strong, partly dispersed waves. It is believed that fully dispersed waves were observed for the first time in a chemically reacting system, in contrast to previous observations involving vibrational non-equilibrium. Finally, it is demonstrated that fully dispersed waves, with their inherently long relaxation lengths and small gradients in state variables, may be used as a particularly simple technique for the chemical kinetic study of flows with one non-equilibrium mode.

CONTENTS

ILLUSTRATIONS

NOMENCLATURE

a	speed of sound (cm/sec)
C_p	specific heat at constant pressure (cal/mole-°K)
d	optical path length (cm)
h	enthalpy (cal/gm)
I	light intensity (arbitrary units)
I_o	incident light intensity (arbitrary units)
k	reaction rate constant (ℓ/mole-sec or ℓ^2/mole^2-sec)
K	equilibrium constant (mole/liter or atmospheres)
ℓ	volume in liters
M	inert gas species
M_s	shock Mach number
p	pressure (torr)
R	universal gas constant (units in text)
t	flow time (shock fixed coordinates)
t_{lab}	laboratory time (laboratory fixed coordinates)
T	temperature (°K)
U	velocity (cm/sec)
V	voltage measured by oscilloscope
W	molecular weight (gm/mole)
x	distance coordinate
X	mole fraction
[i]	molar concentration of ith species (mole/liter)
α	mole fraction of N_2O_4 dissociated
β	mole fraction of O_2 formed
γ	ratio of specific heats

δ slit width (cm)

ε molar extinction coefficient (ℓ/mole-cm)

ξ equal to $(1 - I/I_o)$

ρ density (gm/liter)

τ relaxation time (sec)

SUBSCRIPTS

0 conditions at a point where there is no dissociation of N_2O_4

1 initial conditions in shock tube

2 conditions after translational, rotational and vibrational relaxation, has occured with the chemical reactions frozen

3 conditions after the first chemical reaction ($N_2O_4 \rightarrow 2NO_2$) has reached equilibrium

4 conditions at the final equilibrium state

e equilibrium state

f frozen state

s at constant entropy

SECTION I
INTRODUCTION

At the temperatures achieved in hypersonic flow fields, processes such as vibrational excitation, thermal dissociation, chemical reactions, ionization, radiation, and electronic excitation may occur. In air for example, at Mach numbers above 5, Stupochenko (1) lists six different chemical reactions alone. For the short flow times ordinarily characteristic of high velocity gas dynamics, and in particular at higher altitudes, the assumption that the fluid is everywhere in local thermodynamic equilibrium is not always valid, and the non-equilibrium mechanisms must be included in a description of the flow field.

The large number of simultaneous reactions in air, and the high temperatures required to excite these reactions causes experimental investigations in air to be complicated. In order to investigate certain aspects of the fundamentals of non-equilibrium flow in the laboratory, a different gas system may be chosen in which the temperatures necessary to induce excitation are readily obtainable, and in which the non-equilibrium mechanisms under study may be resolved and uncoupled from each other. For these reasons (2) a flow was chosen in which the following reactions occur:

$$N_2O_4 + M \rightleftarrows 2NO_2 + M \rightleftarrows 2NO + O_2 + M \qquad (1)$$

where M represents an inert gas, either nitrogen or argon. Also, the reactant mole fraction did not exceed 10%. The flow fields were produced in a temperature controlled shock tube in which shock waves of different strengths were propagated through a known equilibrium mixture of the gases of Equation (1).

The work was concerned with three major objectives.

(A) One aim was to investigate the complete picture of a non-equilibrium flow field for shock waves varying from weak, fully dispersed waves to strong, partly dispersed ones. The waves were to be propagated through a gas mixture with a single active non-equilibrium mode whose reaction mechanism and rate constants are well understood.

(B) A second objective was to include a flow field with two non-equilibrium processes. Since the relaxation rate for the second reaction of Equation (1) is much slower than that for the first reaction, these two processes could be experimentally separated.

(C) The third goal was to repeat and extend measurements of the rate constants for both reactions. In particular an extension of results at different temperatures and reactant concentrations than currently available in the literature appeared to be important. Existing rate equations were to be examined in this process and compared with the

results of References 3 through 9.

A shock wave may be defined as a non-equilibrium layer separating two equilibrium states in a gas. As the gas flows through this non-equilibrium layer, molecular collisions change the state of the gas from one equilibrium state to the second. Each degree of freedom of a molecule requires a certain number of collisions to achieve the new equilibrium state. The time required for these collisions to take place is known as the relaxation time and each degree of freedom has its own characteristic relaxation time.

A characteristic time may also be ascribed to the flow. For example, in our flows the time required for a particle to traverse the non-equilibrium layer of a shock wave may be chosen. The ratio of the relaxation time to this particle flow time has often been called the Damköhler parameter D.* For $D \equiv \infty$, the process is frozen since there is no change in the degree of freedom across the region of interest. For $D \equiv 0$, the process is in equilibrium since the degree of freedom relaxes instantaneously. For most applications in flow systems, conditions at these two limits provide an adequate description of the flow fields. However, for situations where $D \approx 1$, non-equilibrium effects must be considered. For the system under consideration in this work,

$$\tau_T, \tau_R \ll \tau_V \ll \tau_\alpha \ll \tau_\beta \qquad (2)$$

in which the subscripts refer to the translational, rotational, vibrational and the two chemical relaxation processes respectively. The translational and rotational modes are here listed together since they are close to each other with respect to the relaxation time for vibrational adjustment.

In the region of interest for the first chemical reaction, the translational, rotational and vibrational degrees of freedom may be considered in equilibrium. In addition, the second reaction is frozen. In the region of interest for the second reaction at higher temperatures, all the other degrees of freedom, including the first reaction may be considered in equilibrium.

An essential feature of a reacting gas mixture is the fact that the mixture behaves as a dispersive medium from the viewpoint of acoustics. There is no unique acoustic velocity and frequency enters as a parameter (11). The acoustic equations for flow with vibrational or chemical non-equilibrium are developed by Vincenti and Kruger (12). Two limiting sound speeds may be defined corresponding to the frozen and equilibrium limits (13). The frozen sound speed a_f propagates as if all processes in the gas were frozen. The equilibrium sound speed a_e which is always less than a_f, (14), propagates as if all processes in the gas were in

*Wegener and Buzyna (10) give some of the history of this parameter and its significance in the description of non-equilibrium flow fields.

equilibrium.

These two limiting sound speeds (12) are expressed as follows. The frozen sound speed a_f is given by

$$a_f^2 \equiv \left(\frac{\partial p}{\partial \rho}\right)_{s,\alpha,\beta} = -\frac{h_\rho}{h_p - \frac{1}{\rho}} \tag{3}$$

where $a_f^2 = \gamma RT$ with $\gamma = C_p/C_v$ if the species are individually thermally perfect. Furthermore, the equilibrium sound speed a_e can be shown to be

$$a_e^2 \equiv \left(\frac{\partial p}{\partial \rho}\right)_{s,\alpha^*,\beta^*} = -\frac{h_\rho + h_\alpha \alpha_\rho^* + h_\beta \beta_\rho^*}{h_p - \frac{1}{\rho} + h_\alpha \alpha_p^* + h_\beta \beta_p^*} \tag{4}$$

Here, the asterisk refers to the equilibrium values of the quantities, and the variables with subscripts indicate partial derivatives. These derivatives were first evaluated by Wegener and Cole (15), specifically for the first reaction of Equation (1). As mentioned first by Bethe and Teller (16) the possibility of shock waves traveling between these two limiting sound speeds exists, and Griffith and Kenny (17) demonstrated the existence of these waves for vibrational relaxation in CO_2.

In this work, these waves were observed for the first time in a chemically reacting system. Waves traveling between the limiting sound speeds were called fully dispersed by Lighthill (18), while waves propagating at velocities above the frozen sound speed were called partly dispersed.

In a partly dispersed wave, there is a normal shock jump in which the rapidly adjusted degrees of freedom relax. In our case they are translation, rotation, and vibration. In this short interval the slow degrees, i.e. the chemical reaction, remains frozen. After the normal shock jump, the slow degrees of freedom proceed to the final equilibrium conditions. As the shock strength is decreased, the overall change in state caused by both the normal shock jump and the chemical reaction decreases. However, the chemical reaction produces an increasing fraction of the total change in state. Finally, for a shock wave propagating exactly at the frozen sound speed, the normal shock jump goes to zero, and the entire change in state is due solely to chemical relaxation. In other words, if the flow velocity is related to the frozen sound speed, at a Mach number of one ($M \equiv U/a_f$) the normal shock vanishes. Below the frozen sound speed, fully dispersed waves provide a continuous transition between the two equilibrium states.

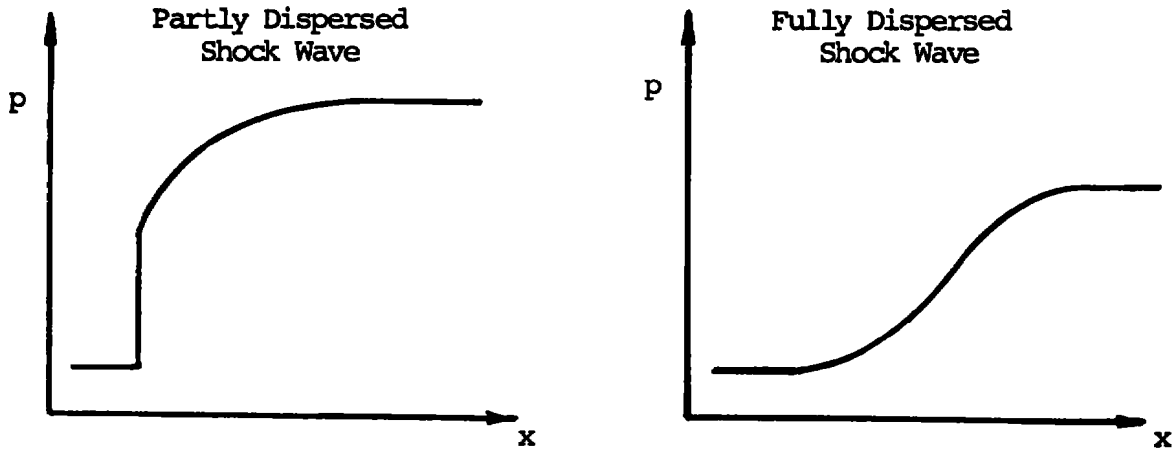

Fig. 1 Schematic Pressure Change for Partly and Fully Dispersed Shock Waves; Flow Direction from Left to Right

Figure 1 shows the typical behavior for pressure of partly and fully dispersed shock waves for an endothermic* reaction. The partly dispersed wave is characterized by the normal shock jump followed by the region of non-equilibrium relaxation. The fully dispersed wave exhibits a continuous non-equilibrium transition between the two equilibrium states, with no normal shock jump apparent.

There are several reasons why the use of fully dispersed waves is ideally suited for a study of chemical kinetics. The chief reason is that the temperature of the reaction can be very accurately determined since the initial temperature of the wave is measured statically. Typically in our work, the total temperature change across the wave is only about ten degrees Kelvin. This accuracy in temperature is important since rate constants are temperature sensitive since they obey laws such as $k = A \exp(-B/T)$ where A and B are constants. Another reason is that the smooth transition between states in these waves facilitates the measurements of slopes. Also, the low velocities and long relaxation times increase the resolution of the experiment. Finally, the small gradients in the flow variables make these waves amenable to simplified theories.

The dispersion owing to the chemical reaction proceeding "slowly" tends to spread the shock wave out in time (or space). This effect is balanced by the convective terms in the conservation equations which tend to steepen the wave. In the steady state, the particles flowing into the shock front pass through the same sequence of states as the preceding ones. The distribution of the variables across the shock front thus forms a fixed picture which moves during this period as an entity together with the front (14).

*Heat is absorbed by the chemical reaction as typically in dissociation.

SECTION II
EQUILIBRIUM PROPERTIES OF THE NITROGEN DIOXIDE SYSTEM AND EQUATIONS OF STATE

The chemical reactions observed in the non-equilibrium flow field were:

$$N_2O_4 + M \rightleftarrows 2NO_2 + M \rightleftarrows 2NO + O_2 + M \tag{5}$$

in which M , an inert component, was either nitrogen or argon.

The mole fractions of the constituents are;*

$$X_{N_2O_4} = \frac{X_o(1 - \alpha)}{1 + \alpha X_o + \beta X_o}$$

$$X_{NO_2} = \frac{2X_o(\alpha - \beta)}{1 + \alpha X_o + \beta X_o}$$

$$X_{NO} = \frac{2X_o\beta}{1 + \alpha X_o + \beta X_o} \tag{6}$$

$$X_{O_2} = \frac{X_o\beta}{1 + \alpha X_o + \beta X_o}$$

and,

$$X_M = \frac{1 - X_o}{1 + \alpha X_o + \beta X_o}$$

In terms of these quantities, the laws of mass action for the reactions are:

---

*In all the equations to be given, values of numerical constants etc. are consistent with the units given in the list of symbols.

$$K_{p1} = p \frac{X_o}{1 + \alpha X_o + \beta X_o} \frac{4(\alpha - \beta)^2}{1 - \alpha} \tag{7}$$

and

$$K_{p2} = p \frac{X_o}{1 + \alpha X_o + \beta X_o} \frac{\beta^3}{(\alpha - \beta)^2} \tag{8}$$

where subscripts 1 and 2 refer to the first and second parts of the reaction respectively.

K_{p1} has been measured by Bodenstein & Böes (6). The results were compiled by Giauque and Kemp (19) and by Strehlow (20). The latter's critical evaluation yields,

$$\log_{10} K_{p1} = - \frac{2989}{T} + 9.187 \tag{9}$$

where T is in degrees Kelvin and the equilibrium constant, K_{p1} in atmospheres pressure.* This part of the reaction takes place in the range $200\ °K < T < 400\ °K$.

The second part of the reaction of Equation (5) was investigated by Bodenstein and Lindner (6) and also compiled by Giauque & Kemp (19). From their data we find in the units of Equation (9):

$$\log_{10} K_{p2} = - \frac{5995}{T} + 7.803 \tag{10}$$

This reaction takes place in the range $500\ °K < T < 1200\ °K$. Much further information including thermodynamic and transport properties is reviewed in References 21, 22 and 23.

At the temperature and relatively low pressures used in the shock tube in the following experiments, the constituents of the gas may individually be considered as thermally perfect gases since intermolecular forces are negligible.

If W, the molecular weight of the mixture is considered as a variable of the non-equilibrium flow field, the thermal equation of state for the mixture becomes

$$\frac{p}{\rho} = \frac{RT}{W} \tag{11}$$

*1 atmosphere = 760 torr.

where R is the universal gas constant. We have:*

$$W = W_M X_M + 92.02\, X_{N_2O_4} + 46.01\, X_{NO_2} + 30.01\, X_{NO} + 32.00\, X_{O_2} \tag{12}$$

The caloric equation of state is

$$h = \frac{1}{W}\left[C_p(T - T_o) + 13846\,\frac{\alpha X_o}{1 + \alpha X_o + \beta X_o} + 27020\,\frac{\beta X_o}{1 + \alpha X_o + \beta X_o}\right] \tag{13}$$

where

$$C_p = X_M\, C_{pM} + X_{N_2O_4}\, C_{pN_2O_4} + X_{NO_2}\, C_{pNO_2} + X_{NO}\, C_{pNO} + X_{O_2}\, C_{pO_2} \tag{14}$$

Values of the specific heats of the constituents and of the heats of reaction were taken from References 24 and 22 respectively.

*With the tabulated values of molecular weights of the National Bureau of Standards.

SECTION III
ANALYSIS OF ONE-DIMENSIONAL NON-EQUILIBRIUM FLOW THROUGH A SHOCK WAVE

The shock tube (25) is a length of tubing divided into two sections by a breakable diaphragm as shown in Figure I.1 in Appendix I, where initially a pressure difference exists between the sections.

Figure 2 is a characteristic x-t diagram of the flow in a shock tube. When the diaphragm is broken, the high pressure driver gas expands into the driven tube. The front of the driver gas, called the contact surface, acts as a piston and drives a shock wave in front of it. A rarefaction wave meanwhile passes through the driver gas and lowers its pressure and temperature. The testing time available at the observation window depends on the lengths of the two tube sections. It is limited by either the passage of the contact surface, the passage of the reflected shock wave, or the passage of the reflected rarefaction wave.

In a shock tube, at a sufficient distance downstream of the diaphragm, the shock wave, across which the variables of state jump and remain fixed relative to each other, propagates at a constant velocity into the quiescent gas in front of it.*

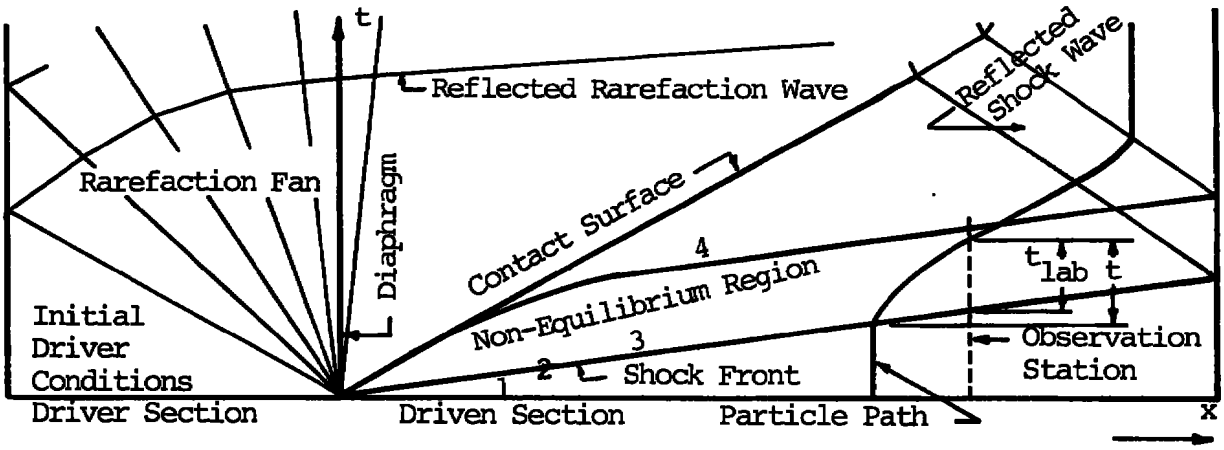

Fig. 2 Characteristic Diagram of Non-Equilibrium Flow in a Shock Tube

In Figure 2, state 1 applies to the initial equilibrium gas mixture at rest. State 2 occurs after the normal shock jump in which the translational, rotational, and vibrational degrees of freedom relax and the chemical reactions are frozen. At state 3 the first reaction of Equation (1) reaches equilibrium while the second reaction is still frozen. Finally, at state 4 all degrees of freedom are again in equilibrium. Typical values of our relaxation times are τ_T , $\tau_R \approx 10^{-3}$ μs , $\tau_v \approx 0.3$ μs ,

*For the actual starting process in a shock tube see Spence (26).

and $\tau_\alpha \approx 10$ μs at $T = 320$ °K and $p = 250$ torr.

In the experiments considered in this work, a temperature range of $280 < T < 2100$ °K and a pressure range of $200 < p < 1000$ torr was investigated. Since the gradients in the flow properties were not great, except in the normal shock jump, the effects of viscosity, heat conduction, and diffusion were neglected. Also, a one dimensional flow approach was valid since boundary layer effects that slow down the shock were shown to be negligible.

In the analysis that follows (36) a coordinate transformation is made in which the shock is fixed while the flow entering the shock front has the measured shock velocity U_1 .

The steady state, one dimensional conservation equations are,

Mass: $$\rho_1 U_1 = \rho' U' \tag{15}$$

Momentum: $$p_1 + \rho_1 U_1^2 = p' + \rho' U'^2 \tag{16}$$

Energy: $$h_1 + \frac{1}{2} U_1^2 = h' + \frac{1}{2} U'^2 \tag{17}$$

The primes denote conditions anywhere in the flow field. For given initial and boundary conditions, these three equations are not sufficient to calculate the four variables ρ , U , p , and h , and an equation of state is necessary to relate these variables. If a gas is in unconstrained thermodynamic equilibrium, two variables are sufficient to describe the thermodynamic state of the medium. For example,

$$h^* = h^* (p, \rho) \tag{18}$$

If the gas is not in equilibrium, then additional variables of state are required for each non-equilibrium mode. The canonical equation of state (12) becomes,

$$h = h (p, \rho, C_p, \alpha, \beta) \tag{19}$$

Here C_p, the specific heat, refers to the translational, rotational and vibrational modes, and α and β refer to the two chemical non-equilibrium degrees of freedom. At equilibrium, Equation (19) reduces to Equation (18) since the non-equilibrium variables become functions of p and ρ alone. The caloric and thermal equations of state for the gas system under consideration

are given by Equations (13) and (11).

These equations together with the conservation equations and for the given initial conditions of p_1 , ρ_1 , U_1 , and h_1 are sufficient to solve the flow conditions at the states 2, 3, and 4 of Figure 2.

State 2 occurs after the normal shock jump in which the translational, rotational, and vibrational degrees of freedom adjust. As a first approximation to this state, C_p , α , and β are frozen and the caloric equation of state for a thermally perfect gas becomes simply,

$$h' = \frac{1}{W} C_{pl} T' \tag{20}$$

where the reference enthalpy, h_1 , has been set equal to zero. The solution of Equations (15), (16), (17), (11) and (20) represents the well-known Rankine-Hugoniot solution (27) for a thermally and calorically perfect gas, and one obtains p' , ρ' , U' , and h' . We define,

$$\bar{C}_p \equiv \frac{1}{T_2 - T_1} \int_{T_1}^{T_2} C_p \, dT \tag{21}$$

where C_p is the relaxed heat capacity at T . With this, the caloric equation of state becomes,

$$h_2 = \frac{1}{W} \bar{C}_p \, (T_2 - T_1) \tag{22}$$

Setting h_2 equal to h' initially, Equations (15), (16), (17), (11) and (22) can be solved by iteration to obtain the conditions for state 2.

At state 3, the first reaction of Equation (1) goes to equilibrium while the second reaction is considered to remain frozen. To obtain conditions at this point the law of mass action, Equation (7), is employed. From Equations (7) and (9), the degree of dissociation is calculated for particular values of pressure and temperature. Initial values of state 3 are assumed, and with Equation (7) the Equations (15), (16), (17), (11) and (13) may again be solved by iteration to obtain conditions for state 3.

The final state 4 occurs after all degrees of freedom have relaxed to their equilibrium values. The law of mass action for the second reaction of Equation (1) is Equation (8). This equation together with Equations (7), (15), (16), (17), (11) and (13) are again solved by iteration to obtain conditions for state 4.

For the fully dispersed wave, state 1 and 2 are equivalent; that is, there is no normal "shock jump". Since the initial temperature T_1 was low in our experiments and since fully dispersed waves are weak, the second reaction was not excited, and states 3 and 4 therefore coincided.

In order to describe the non-equilibrium flow field in detail, it is necessary to know the time dependent behavior of the non-equilibrium variables of state. These relationships are given by the rate equations. Both reactions of Equation (1) have been previously investigated and the reaction mechanisms appear to be known. These two rate equations are discussed in Section VI. Utilizing the thermal equation of state (11), with the relationships of Equation (6), the two coupled rate equations (61) and (68) can be rewritten as,

$$\frac{d\alpha}{dt} = k_{D1} \frac{p}{RT} \left[(1 - \alpha) - \frac{p}{K_{p1}} \left(\frac{4X_o(\alpha - \beta)^2}{1 + \alpha X_o + \beta X_o} \right) \right] \tag{23}$$

and

$$\frac{d\beta}{dt} = k_{D2u} \frac{p}{RT} (\alpha - \beta) + k_{D2b} \frac{p}{RT} \frac{2X_o(\alpha - \beta)^2}{1 + \alpha X_o + \beta X_o} + \frac{d\alpha}{dt} \tag{24}$$

The one dimensional steady state conservation equations, differentiated with respect to time in a shock fixed coordinate system are,

Mass:
$$\rho \frac{dU}{dt} + U \frac{d\rho}{dt} = 0 \tag{25}$$

Momentum:
$$\frac{dp}{dt} + \rho U \frac{dU}{dt} = 0 \tag{26}$$

Energy:
$$\frac{dh}{dt} + U \frac{dU}{dt} = 0 \tag{27}$$

It is noted, that conditions are fixed at a given time or distance downstream of the normal shock jump, and the time dependence of the variables is a function of position from the shock front.

Differentiating the thermal equations of state (11) logarithmically yields

$$\frac{dp}{p} + \frac{dW}{W} - \frac{d\rho}{\rho} - \frac{dT}{T} = 0 \tag{28}$$

where

$$\frac{dW}{W} = - \frac{X_o(d\alpha + d\beta)}{1 + \alpha X_o + \beta X_o} \tag{29}$$

and

$$\frac{1}{p}\frac{dp}{dt} - \frac{X_o}{1 + \alpha X_o + \beta X_o}\left(\frac{d\alpha}{dt} + \frac{d\beta}{dt}\right) - \frac{1}{\rho}\frac{d\rho}{dt} - \frac{1}{T}\frac{dT}{dt} = 0 \tag{30}$$

From the caloric equation of state, (13),

$$\frac{dh}{dt} = \left(\frac{\partial h}{\partial T}\right)_{\alpha,\beta}\frac{dT}{dt} + \left(\frac{\partial h}{\partial \alpha}\right)_{T,\beta}\frac{d\alpha}{dt} + \left(\frac{\partial h}{\partial \beta}\right)_{T,\alpha}\frac{d\beta}{dt} \tag{31}$$

where the partial derivatives, evaluated from Equation (13) are,

$$\left(\frac{\partial h}{\partial T}\right)_{\alpha,\beta} = C_p \tag{32}$$

$$\left(\frac{\partial h}{\partial \alpha}\right)_{T,\beta} = \frac{X_o}{W(1 + \alpha X_o + \beta X_o)^2}(13846 - 13174\ \beta X_o) \tag{33}$$

and

$$\left(\frac{\partial h}{\partial \beta}\right)_{T,\alpha} = \frac{X_o}{W(1 + \alpha X_o + \beta X_o)^2}(27020 + 13174\ \alpha X_o) \tag{34}$$

Finally,

$$\frac{dx}{dt} - U = 0 \tag{35}$$

where x is distance measured behind the shock front.

In the fixed shock coordinates used, the time t is the flow time. This is the time for a particle to travel from the shock front to some position x downstream. In the laboratory, however, time is measured from the passage of the shock front across the observation window till the

passage of a particle a distance x behind the shock front. This time, t_{lab}, is equal to;

$$t_{lab} = \frac{x}{U_1} \tag{36}$$

where U_1 is the shock velocity.

These two times are related through Equations (35) and (36) and Figure 2 graphically demonstrates the difference between these two times. It is seen that $t > t_{lab}$. This causes a time "compression" on oscilloscope traces since such observations of e.g. pressure, record changes of state at a fixed location in the shock tube.

Equations (23) through (27), (30), (31) and (35) comprise eight coupled first order non-linear equations in the variables α, β, ρ, U, p, h, T, and x. These equations were numerically integrated on an IBM 7090-7094 DCS computer using Milne's second-difference method with a Hamming Predictor-Corrector. (References 28, 29).

The initial conditions for these eight equations come from the measured values of X_o, p_1, T_1 and U_1 from which α_1, β_1, ρ_1 and h_1 are calculated. The integration is carried out until α and β are within one percent of their equilibrium values at state 4. Since the flow variables asymptotically approach their final values, the relaxation time literally goes to infinity. It is physically more meaningful therefore to ascribe a value to τ when the reaction has reached a certain stage near the final equilibrium state. For this work, τ was arbitrarily taken as the time when α and β have reached 99% of their final values, therefore,

$$\tau_\alpha \equiv t_\alpha = 0.99\ \alpha_4$$

and (37)

$$\tau_\beta \equiv t_\beta = 0.99\ \beta_4$$

For a fully dispersed wave, the initial conditions are the values at state 1. A difficulty arises since this is an equilibrium state and the right hand side of Equation (23) is equal to zero. Hence, α will not progress to its value at state 4. A computational device was used to overcome this. The initial conditions were perturbed slightly and the integration then proceeded. The perturbation consisted of adding 10^{-6} to the initial value of α. The effect of this perturbation was shown to be negligible by doubling the perturbation in the calculation with no appreciable effect noted in the result.

As discussed by Vincenti and Kruger (12) a continuous solution for a partly dispersed wave does not exist if the initial conditions are chosen as those of state 1. Therefore, a discontinuity in the flow variables resulting in the conditions at state 2 provides the initial conditions for this case and the equations may then be integrated to the final conditions at τ_α and τ_β .

The concentration of NO_2* is,

$$[NO_2] = \frac{p}{RT} \frac{2X_o(\alpha - \beta)}{1 + \alpha X_o + \beta X_o} \tag{38}$$

From this relationship, the ratio of the concentration of NO_2 at any point in the flow field to the initial concentration of NO_2 is obtained. These values are compared to the experimental values in Section VII. Also, the calculated values for several experiments of α , β , T/T_1 , p/p_1 and U/U_1 vs. t are given.

*We recall the definition of concentration given by $[i] = \frac{p_i}{RT} = \frac{p}{RT} Xi$

SECTION IV
EXPERIMENTAL EQUIPMENT AND METHODS

Figures I.1 and I.2 in Appendix I show a sketch and a photograph of the shock tube, chemical mixing station, and instrumentation. The shock tube is 28 feet long overall, with an inside diameter of 3 inches. The driver section is 4 feet long and the entire tube is constructed of stainless steel to permit the use of the highly corrosive nitric oxides. A jacket surrounds the tube so that the walls may be heated or cooled by circulation of suitable liquids. Thermocouples monitor the temperature along the tube length. Shock speeds are measured by timing the shock passage between two optical trigger stations. These stations use an "absorption" trigger for weak shocks and a conventional schlieren type trigger for stronger shock waves. Between these two stations is the light absorption station which measures the time dependent concentration of NO_2. In the mixing station, the reactant gases and the inert gas are introduced into a cylinder in which they are thoroughly mixed prior to introduction into the shock tube. A detailed description of the equipment is given in Appendix I.

To determine the non-equilibrium flow through a shock wave, it is necessary to find the initial conditions of the flow variables entering the wave and the time dependent history of the non-equilibrium relaxation processes.

A gas mixture is prepared as described in Appendix I, giving the initial reactant mole fraction X_o. This mixture enters the shock tube where the pressure is recorded to ± 0.1 torr and the temperature to ± 0.1 °K. The shock velocity is measured by timing the shock passage between two trigger stations as described in Appendix I. Using this technique the shock velocity is known to better than 0.3%. The initial conditions X_o, p_1, T_1, and U_1 are thus determined.

The time dependent concentration of one species of the reaction, $[NO_2]$, was furthermore measured photometrically to determine the non-equilibrium mode. The absorption spectra of N_2O_4 and NO_2 are given by Hall and Blacet (30) and it is found that at 4350 Å, NO_2 absorbs strongly while N_2O_4 is transparent. The inert gases nitrogen or argon are, of course, also transparent at this wave length as is NO. Figure 3 is a plot of I/I_o vs. $[NO_2]$ with I/I_o as the ratio of transmitted to incident light. A linear relationship between the concentration and the logarithm of I/I_o is observed. Lambert-Beer's law is therefore experimentally validated and we can write

$$\frac{I}{I_o} = 10^{-\varepsilon [NO_2] d} \tag{39}$$

where d is the optical path length.

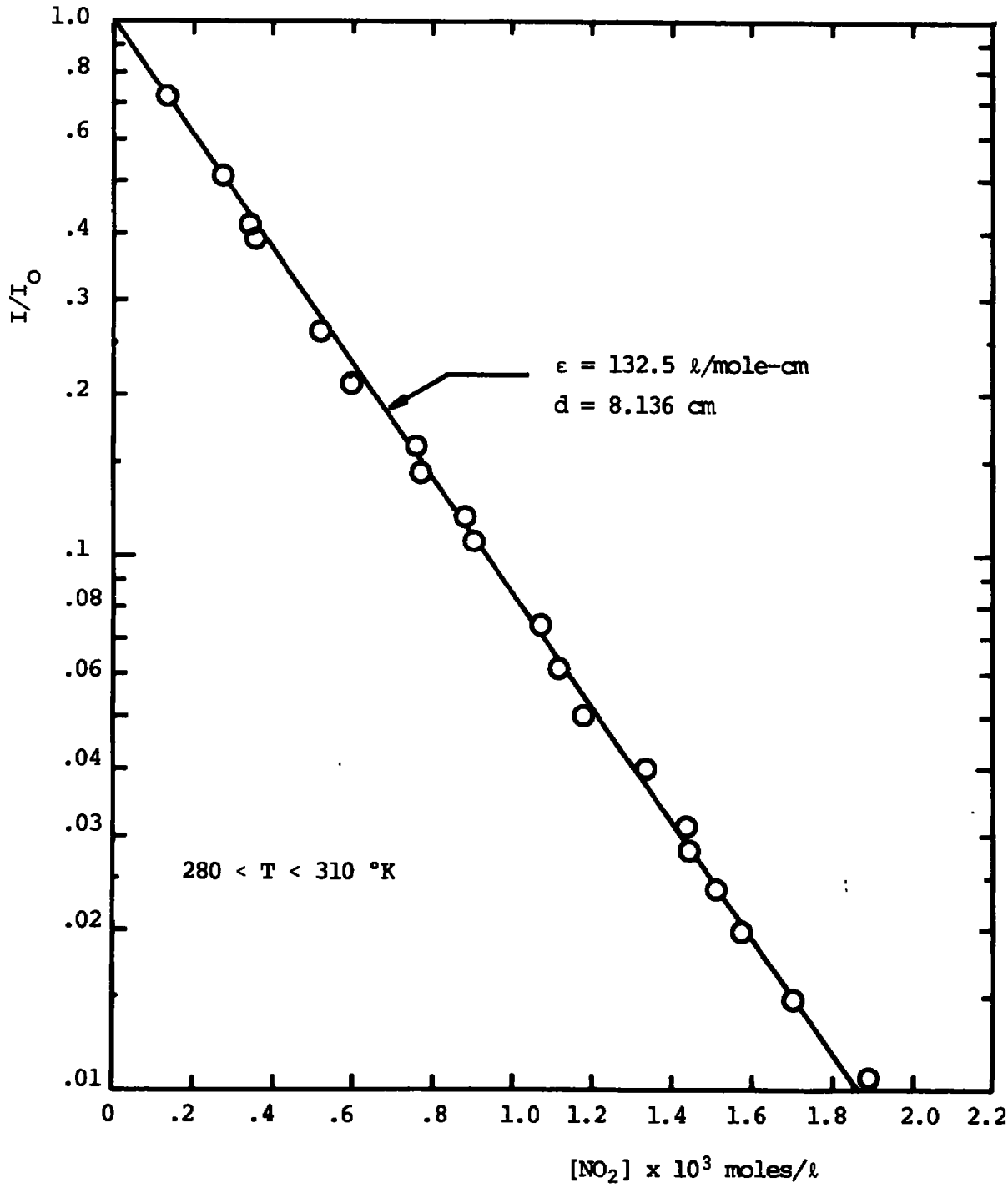

Fig. 3 Intensity Ratio versus NO_2 Concentration
$\epsilon = \log_{10} (I_o/I/[NO_2]\ d$

Over the large temperature range investigated in this work ($280 < T < 2100$ °K), the molar extinction coefficient, ε, was found to have a small temperature dependence. However, within the small temperature changes induced by the weak shock waves utilized in investigating flow fields with only one non-equilibrium mode, i.e. the dissociation of N_2O_4, the value of ε was taken to be constant.

Using the slope of the line in Figure 3 and Equation (39), a value of ε is obtained, and

$$\varepsilon = 132.5 \text{ ℓ/mole-cm} \tag{40}$$

in the temperature range $280 < T < 310$ °K. These measurements were made directly in the shock tube, with I and I_o measured as explained in Appendix I, and with $[NO_2]$ calculated from Equation (38). Since all reactions are very rapid, the system remains at equilibrium during gas handling operations making the measurements valid as described. This value is in agreement with that of Wegener (4). A series of neutral density filters was employed to investigate the possibility of photo-dissociation. It was found that by successively reducing the incident light intensity, I_o, by a factor of two, the output signal, I, also varied by the same factor so that I/I_o remained constant. Since photo-dissociation would have varied I/I_o as a function of I_o, the constant ratio of I/I_o showed photo-dissociation to be negligible.

At the higher temperature interval ($T > 1200$ °K) in which the second part of reaction (1) takes place the temperature dependence of ε could no longer be neglected. Also, ε could not be measured directly as it could at room temperature. This is due to the fact that NO_2 is unstable at these temperatures. Therefore, an indirect approach, based on the kinetic record of the dissociation was employed to find the molar extinction coefficient. In the following relation;

$$\frac{V_3}{V_1} = \frac{I_3/I_o}{I_1/I_o} \tag{41}$$

V_1 and V_3 are the measured voltages at states 1 and 3 respectively. I_1/I_o is the transmitted to incident light ratio at state 1, and I_3/I_o may then be determined. State 3 corresponds to the maximum concentration of NO_2 as described in Section VII.

From the analysis of Section III, $[NO_2]_3$ can be calculated at temperature T_3. Now using Equation (39) a value of ε is achieved for a specific temperature.

Figure 4 is a plot of ε vs. T from a series of experiments using a variety of conditions of state 3. The lack of dependence of ε on

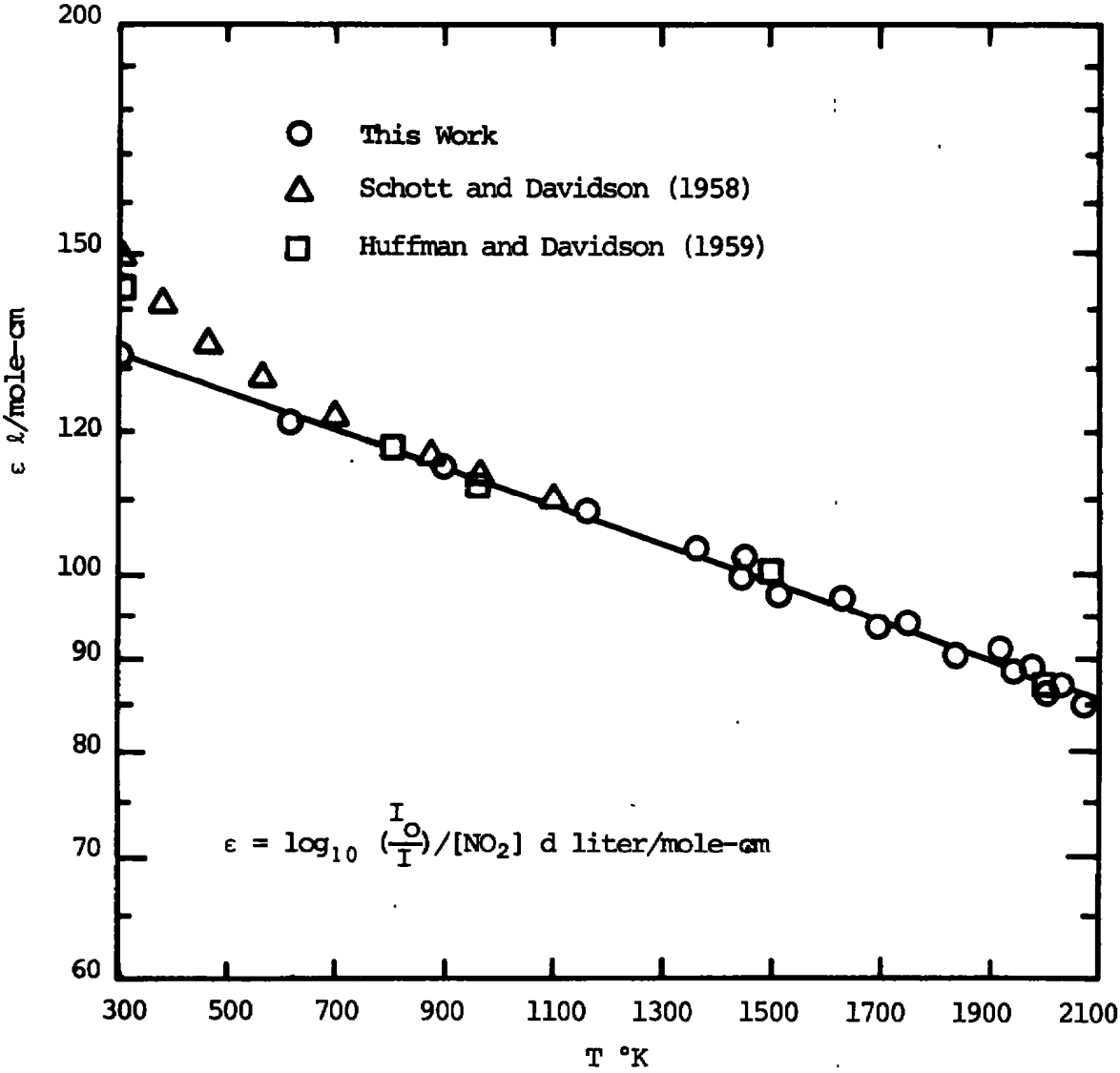

Fig. 4 Temperature Dependence of the Extinction Coefficient at 4350Å

concentration of NO_2 is evidence that Lambert-Beer's law is still valid at the higher temperatures. The values of Schott and Davidson (31), and Huffman and Davidson (8) agree well with this work. The results shown in Figure 4 may be represented by the relationship

$$\log_{10} \varepsilon = - 1.113 \times 10^{-4} T + 2.161 \tag{42}$$

for a range of temperatures $300 \leq T \leq 2100$ °K.

This method of obtaining ε has the effect of forcing the theoretical and experimental values of $[NO_2]$ to coincide at state 3. For the low temperature results of the first reaction of Equation (1) this was not the case since ε was determined independently of the analysis. In Section VII, it will be seen that the theoretical and experimental values for conditions at state 2 compare well for the first reaction. This would indicate that the prediction of conditions at state 3 for the second reaction essential for the measurement of $\varepsilon(T)$ may also be assumed to be reliable.

In the photometric measurement of the NO_2 concentration a narrow parallel beam of light is employed. This beam passes at right angles to the tube wall through the gas mixture and impinges upon the photomultiplier tube. The accuracy of these measurements depends upon two factors, the electronic response time of the photomultiplier system, and the width of the parallel light beam. The electronic response time of the photomultiplier system used was measured to be less than 0.5 μs (see Appendix I) and therefore it is much more rapid than the phenomena that concern us here.

In Section I the concept of the Damköhler parameter was introduced as the ratio of the relaxation time to a characteristic flow time. Similarly, a Damköhler parameter may be defined in terms of the ratio of a relaxation length to a flow length. The appropriate flow length for the measurements made in this system is the slit width of the light absorption measuring system. The slit width was here chosen to be large enough so that $D << 1$ (equilibrium) was valid for translational, rotational, and vibrational relaxation. On the other hand the slit width was chosen to be small compared to the chemical relaxation length.

The effect of the slit width on such measurements is discussed by Stupochenko (1). With a finite width, δ, the signal, V, measured at any given instant is an average of the actual signal, I, over the slit width so that

$$V = \frac{U_1}{\delta} \int_{t - \delta/2U_1}^{t + \delta/2U_1} I \, dt \tag{43}$$

If the signal, I, is approximated by an exponential,

$$I = I_o \exp\ (-t/\tau) \tag{44}$$

where τ is a chemical relaxation time, then,

$$V = \frac{2\tau I_o U_1}{\delta} e^{-t/\tau} \sinh \frac{\delta}{2U_1\tau} \tag{45}$$

This equation may be expanded in a series to yield

$$V = I_o e^{-t/\tau} \left(1 + \frac{\delta^2}{24\ U_1^2\tau^2} + \ldots\ldots\right) \tag{46}$$

The effect of the slit width will be negligible if the following condition holds:

$$\frac{\delta^2}{24\ U_1^2\tau^2} << 1 \tag{47}$$

In our experiments the slit width was 0.6 mm and if an extreme example of the results to be shown later is considered, values of $U_1 = 356$ m sec^{-1} and $\tau = 3$ μs may be assumed. For this situation, the term on the left hand side of Equation (47) is equal to 0.013. This value may be considered negligible compared to one. For the above shock speed, the time required for the shock front to pass across the slit is equal to 1.7 μs. At 320 °K, the vibrational relaxation time for N_2O_4 is 0.3 μs (32,33). The Damköhler parameter for vibrational relaxation is therefore equal to 0.18. This value of D is sufficiently small to justify the assumption of vibrational equilibrium as stated at the beginning of the discussion of the effect of the slit width. The more rapidly adjusted degrees of freedom of rotation and translation will achieve equilibrium in an even shorter period of time.

SECTION V
EXPERIMENTAL RESULTS

The non-equilibrium flow fields were experimentally investigated using the following technique. A gas mixture with a prescribed mole fraction of N_2O_4 at a point where there is no dissociation, X_o, was prepared. This mixture was admitted to the shock tube at a measured p_1 and T_1. From these values, the frozen sound speed a_{f1} of the mixture was computed by Equation (3). A shock wave was propagated through this gas mixture and its velocity U_1 was measured, giving the shock Mach number $M_s = U_1/a_{f1}$. As shown in Figure 5, oscilloscope traces of voltage versus time are obtained in which the voltage is proportional to the transmitted light intensity. From these traces, and from the previously measured value of I_o, the time dependent NO_2 concentration may be computed using Equation (39).

In light of the objectives of this work, the experiments were divided into two groups: weak shock waves in which only one non-equilibrium degree of freedom was excited; and shock waves with two non-equilibrium degrees of freedom.

Figure 5 shows oscilloscope traces for fully dispersed and partly dispersed shock waves propagating through a gas mixture of N_2O_4, NO_2, and A. In all these experiments, the conditions at state 1 were the same, and the shock strengths were varied by changing the pressure in the driver section of the shock tube. In these experiments the voltage which is directly proportional to light intensity, is inverted so that the positive direction corresponds to NO_2 concentration or to α, the progress variable or degree of dissociation. The first three experiments (506, 505, and 504) give results for fully dispersed shock waves and it is believed that they represent the first demonstration of these waves for a chemically relaxing system. The continuous transition from equilibrium state 1 to the final equilibrium state is clearly seen. The next six experiments involve partly dispersed shock waves. These waves continuously increase in strength as seen in the traces for experiments 503, 500, 498, 497, 494 and 496. Partly dispersed waves are characterized by a normal shock jump across which only the translational, rotational, and vibrational degrees of freedom equilibrate. This shock jump is followed by the chemical relaxation of the first reaction of Equation (1) to its final equilibrium value. If the shock waves are looked at in order of decreasing shock strength, it is seen that as predicted before, the normal shock jump decreases in proportion to the total change of state. At waves propagating at the frozen sound speed, a_{f1}, the normal shock jump goes to zero. Utilizing the methods of Section III, conditions can be measured at state 1, the initial conditions and computed at state 2, conditions after the normal shock jump, and at state 4, conditions at the final equilibrium state. These values are presented in Table II.1 of Appendix II for the nine experiments of Figure 5. In Figures 12, 13 and 14 in Section VII, the calculated concentration ratios with respect to conditions at state 1 are compared to the experimental concentrations obtained using Equation (39). The agreement is seen to be good.

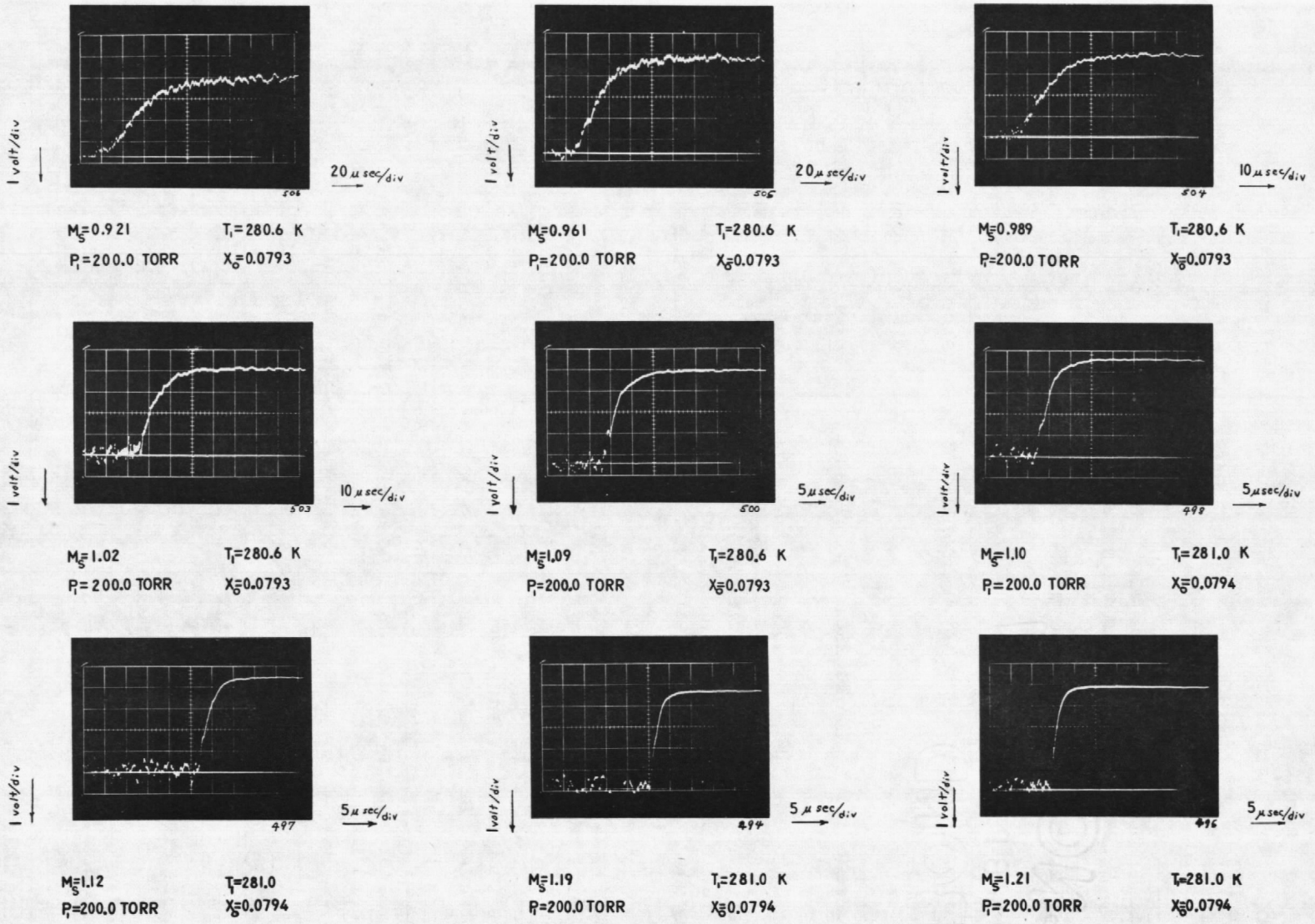

Fig. 5 Fully Dispersed and Partly Dispersed Shock Waves in N_2O_4 - NO_2 - A at Same Initial Conditions

The second series of experiments is concerned with shock waves strong enough to raise the temperature sufficiently to cause the dissociation of NO_2 in the second reaction of Equation (1). In these experiments it was found expedient to vary the initial pressure, p_1 , in the shock tube. This had the effect of keeping the pressure fairly constant after the normal shock jump. Figure 6 shows oscilloscope traces for these strong shock waves for two series of experiments using gas mixtures of different X_O . As reported in Huffman and Davidson (8), an orange light glow was at first observed to emanate from the shock tube for these strong shock waves. Since the carrier gas itself and the reacting gas were not nearly hot enough to radiate at the shock strengths observed, and since no explanation of this phenomenon was available, work was performed to determine the origin of the glow.

At first, experiments carried out with pure argon, nitrogen and helium omitting the reactants also showed this glow. This demonstrates that the glow clearly was not caused by the reacting gas. Experiments with stronger shocks, up to $M_S = 8$ showed a color shift of the radiation to the blue indicating a continuum black body radiation. Calculations on the heat transfer through the boundary layers though, showed that the walls of the tube were not heated above 100 °C and therefore did not radiate. By inserting a carefully cleaned glass tube into the shock tube, the possibility of radiating scale or grease on the walls was also eliminated. Experiments were then performed in which the vacuum pump was cold trapped, and research grade gases of high purity were used. In these experiments the radiation was greatly reduced and the radiation effect was therefore shown to be caused by the organic impurities, such as pump oil, present in the tube.

In the experiments shown in Figure 6, the 4350 Å absorption filter and a series of collimating slits were placed between the photomultiplier tube and the shock tube window. In this configuration with the research grade gases, no radiation was detectable and the effect was eliminated.

In Figure 6, voltage is again shown as in Figure 5 and in experiments 577 to 567 the effects of increasing the shock strengths are seen. A normal shock jump occurs across which the translational, rotational, and vibrational degrees of freedom, and the first chemical reaction equilibrate. Following the normal shock jump the second chemical reaction is observed. As the shock strength increases, as expected the rate of dissociation of NO_2 is seen to increase. Therefore NO_2 disappears and consequently the light absorption decreases. In experiment 577, the oscillations at the end of the trace can be shown to be due to the arrival of the contact surface. This was not observed in the other experiments which were taken at higher sweep speeds. Experiments 587, 590, 596 and 599 show a similar trend of dissociation for a gas mixture at a lower value of X_O .

In Table II.2 of Appendix II, a number of parameters are shown which were calculated for these nine experiments. We recall that state 1 corresponds to the initial measured conditions. At state 2, the translational, rotational, and vibrational degrees of freedom are in equilibrium, while the chemical reactions are frozen. At state 3, two sets of conditions are given:

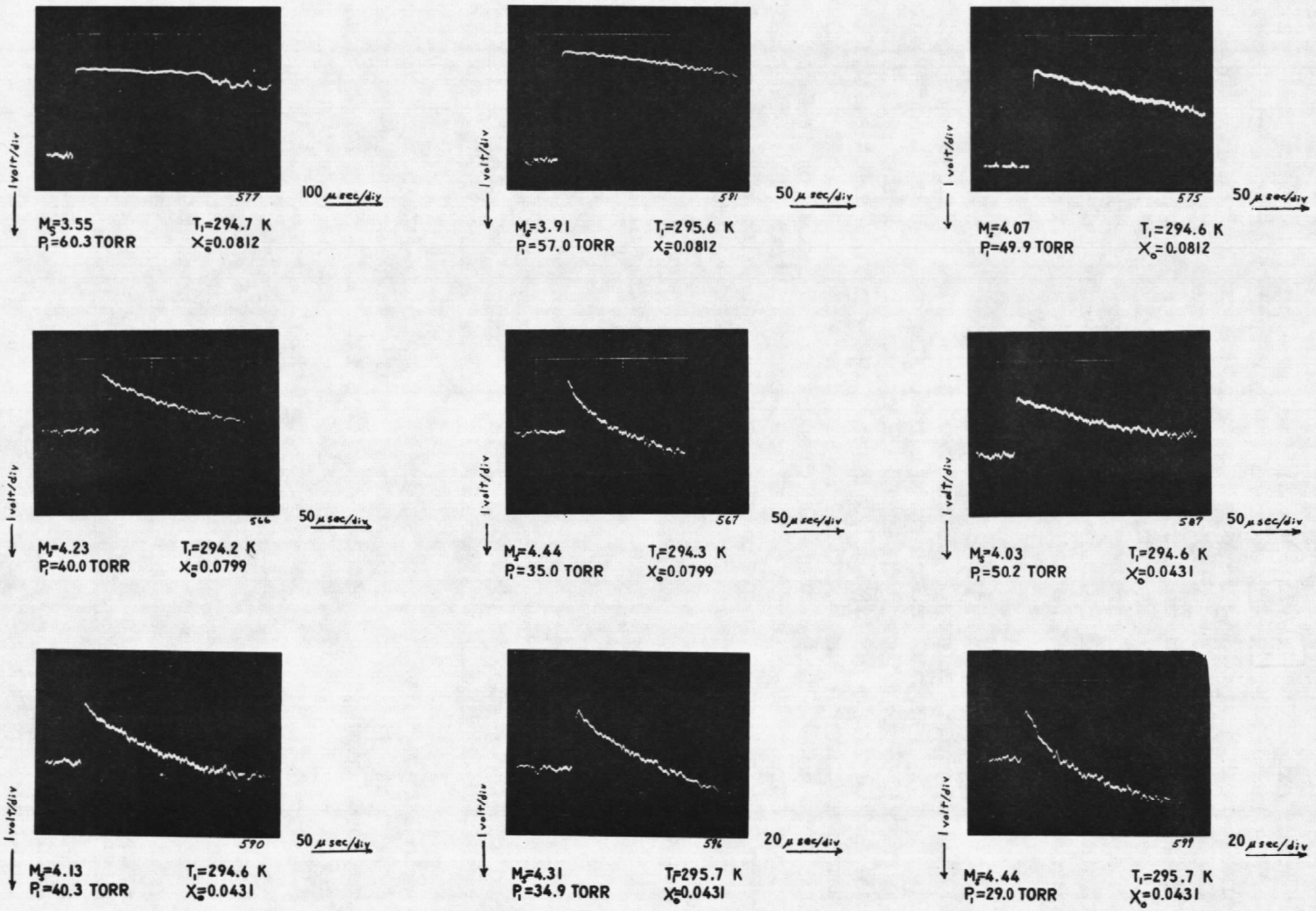

Fig. 6 Strong Shock Waves in N_2O_4 - NO_2 - A for two Different Reaction Mole Fractions

the conditions at which the second reaction is frozen while the first reaction goes to equilibrium, and the conditions at which the second reaction proceeds while the first reaction goes to equilibrium. This second set of values corresponds to the maximum NO_2 concentration observed. Finally, state 4 is the conditions for final equilibrium. Figure 18 shows the experimental versus the theoretical values of the NO_2 concentration ratio versus x, the distance downstream of the normal shock front.

SECTION VI
CHEMICAL KINETICS

At this point, all experimental parameters have been measured or computed and this section is concerned with a study of the chemical reactions of Equation (1) as inferred from the results. For the two reactions, the relationship $\tau_\alpha << \tau_\beta$ is valid as will be demonstrated in Section VII and therefore, the two reactions can be uncoupled. In the analysis that follows, β is considered frozen in the first reaction which takes place at temperatures below 400 °K. In turn for the second reaction, at temperatures above 600 °K, α is in equilibrium.

A rate equation for a chemical reaction may be of the general form

$$\left(\frac{\partial \alpha}{\partial t}\right)_T = k_D \, f(p, T, \alpha) \tag{48}$$

where the derivative on the left hand side refers to the fact that the reaction is forced to take place at a constant temperature. In such an environment k_D represents a constant. However, if the reaction does not take place at a constant temperature, which is the case for this work, the temperature dependence of the rate "constant" k_D must be considered. If a rate equation is of the form of Equation (48), then the coefficient, k_D, may be found from the oscilloscope traces which give the time rate of change of the concentration of NO_2 with respect to a fixed observation point in the shock tube. The following procedure was used to determine k_{D1} as defined by Equation (23). It is seen that this equation is furthermore of the form of Equation (48). Later in this section, Equation (23) will also be shown to be the rate equation for the first reaction of Equation (1). If we define a parameter

$$\xi = 1 - I/I_o \tag{49}$$

then:

$$\frac{d\alpha}{dt} = \frac{d\xi}{dt} \Big/ \frac{d\xi}{d\alpha} \tag{50}$$

Laboratory time is related to the flow time by Equations (35) and (36) to give

$$\frac{dt}{dt_{lab}} = \frac{dx/dt_{lab}}{dx/dt} = \frac{U_1}{U} \tag{51}$$

$$\frac{dh}{d\alpha} = C_p \frac{dT}{d\alpha} + \left(\frac{\partial h}{\partial \alpha}\right)_{T,\beta} \tag{59}$$

Equations (54) to (59) form a set of six first order differential equations which may be numerically solved to give values of $d\xi/d\alpha$, ξ , p , T , and U as functions of α . Now using Equations (52) and (48), values for k_D are finally obtained as a function of temperature.

For the second reaction involving the dissociation of NO_2, the rate equation is more complex and contains terms expressing two competing mechanisms, as seen in Equation (24). These two mechanisms are a unimolecular and a bimolecular process. Since $\tau_\beta >> \tau_\alpha$, α remains at its final equilibrium value throughout the second reaction, and the rate equation has the form

$$\left(\frac{\partial \beta}{\partial t}\right)_T = k_{D2u} f_1 (p, T, \beta) + k_{D2b} f_2 (p, T, \beta) \tag{60}$$

The procedure used in obtaining these two rate constants is as follows: The derivatives in Equations (52) and (54) to (59) are rewritten with respect to β instead of α . These equations are again solved numerically to give values of $d\xi/d\beta$, β , p , T , and U as functions of β . Two limiting cases may now be calculated from Equation (60). In the first case, k_{D2b} is set equal to zero so that the rate equation reduces to the form of Equation (48). Now using the β equivalent of Equation (52) and the first term on the right hand side of Equation (60), values for k_{D2u} are obtained. Similarly, k_{D2u} may be set equal to zero as the other limiting case and, in turn, values of k_{D2b} may be obtained.

The physical significance of the results obtained by these methods will be discussed next. Both of the chemical reactions in Equation (1) have been extensively investigated in certain ranges and the reaction mechanisms appear to be well known. The pioneering work on the first reaction was done by Carrington and Davidson(3). It is interesting to note that the study of this reaction represented the first application of a shock tube to research in chemical kinetics. The dissociation rate constant was found in a manner similar to that employed here. Wegener (2) utilized the inverse technique, i.e. the cooling of the gases in a supersonic nozzle to measure the recombination rate constant in the first application of supersonic nozzles to studies of chemical kinetics. Other work on this reaction was performed by Bauer and Gustavson (33) who measured relaxation times in a Kantrowitz type impact tube, and by Sessler (34) and Cher (5) who measured the dissociation rate constant using the classical method of ultrasonic absorption.

The different techniques mentioned have given results in good agreement and the rate equation deduced from the experiments is given by,

$$\left(\frac{\partial [N_2O_4]}{\partial t}\right)_T = - k_{D1} [N_2O_4][M] + k_{R1} [NO_2]^2 [M] \tag{61}$$

Here, the brackets denote concentration and M stands for any molecule participating in the reaction. Furthermore, k_{D1} and k_{R1} denote the dissociation and recombination rate constants respectively. At equilibrium, $\partial[N_2O_4]/\partial t \equiv 0$, and the right hand side of Equation (61) reduces to the law of mass action (7) so that

$$\frac{k_{D1}}{k_{R1}} = K_{C1} = \frac{K_{p1}}{RT} \tag{62}$$

Here, k_{D1} has units of liters mole^{-1} sec^{-1}, k_{R1} has units of liters^2 mole^{-2} sec^{-1} so that the equilibrium constant K_{C1} has units of mole liter^{-1}. K_{p1} has units of atmospheres so that the universal gas constant is $R = 0.08205$ liter atm. mole^{-1} °K^{-1}. Reaction (61) exhibits a second order rate of dissociation and a third order recombination rate.* The dissociation rate constant was measured using oscilloscope traces similar to those of Figure 5. Utilizing the measured values of ξ and $d\xi/dt_{lab}$ obtained from these traces, k_{D1} was calculated by the methods presented above.

Figures 7 and 8 are plots of k_{D1} vs. $1/T$ for inert gases of nitrogen and argon respectively. The data is seen to fit the Arrhenius equation:** For N_2

$$k_{D1} = 2.85 \times 10^{14} \exp(-11{,}000/RT) \text{ ℓ/mole-sec} \tag{63}$$

and for A ;

$$k_{D1} = 2.23 \times 10^{14} \exp(-11{,}000/RT) \text{ ℓ/mole-sec} \tag{64}$$

Here, as is customary $R = 1.987$ cal mole^{-1} °K^{-1} .

These results, in accord with those of Cher show that nitrogen was more efficient in causing a reaction than argon. The results of this work are seen to be in good agreement with those of Carrington and Davidson (3), and Cher (5). Employing Equation (62) recombination rate constants may be calculated from the measured k_D and the known K_C . These results are

---

*We recall that the order of a reaction may be inferred by adding the exponents in the concentration terms.

**In equations such as (63) and (64), the exponential constant refers to the activation energy. The pre-exponential term is a function of the collision rate, and the probability that a sufficiently energetic collision will actually result in a reaction. This last term is also known as the steric factor (35).

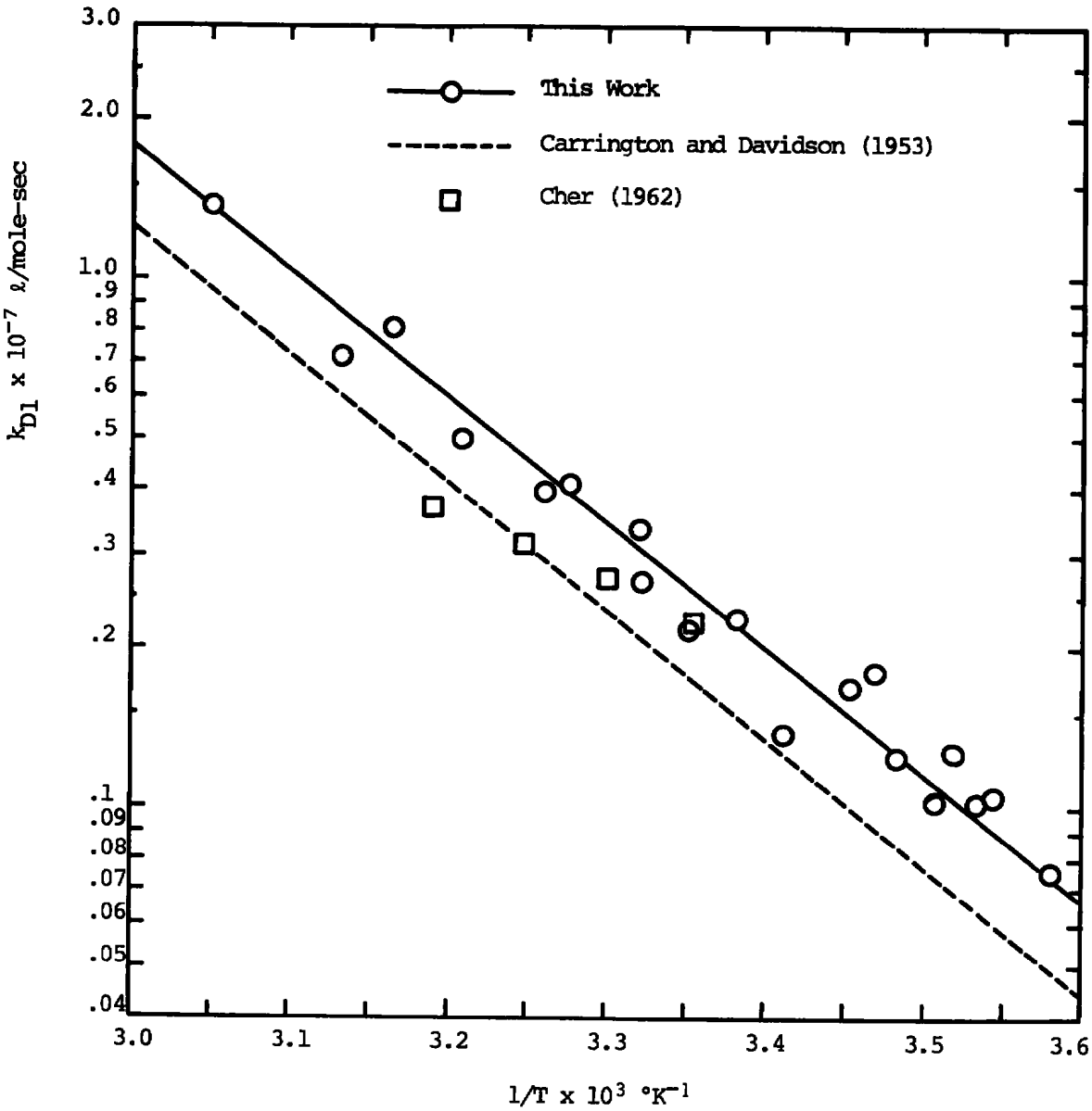

Fig. 7 Dissociation Rate Constant versus 1/T for $N_2O_4 + N_2 \rightleftharpoons 2NO_2 + N_2$

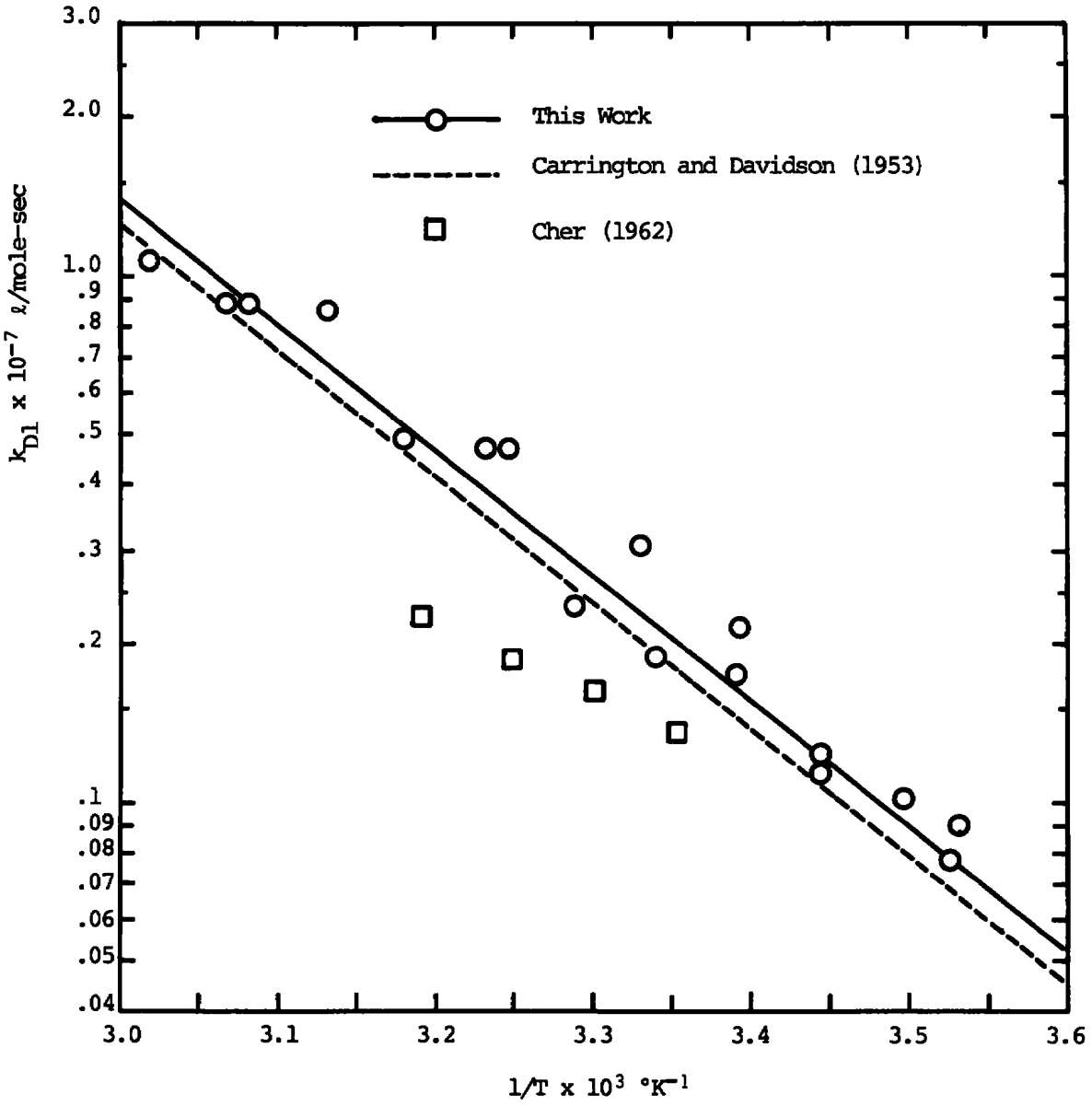

Fig. 8 Dissociation Rate Constant versus 1/T for $N_2O_4 + A \rightleftharpoons 2NO_2 + A$

plotted vs. temperature in Figure 9 and agreement with the measurements of Wegener (2) is found. We note that k_{R1} is plotted on a linear scale emphasizing the customary scatter of such findings.

The original work on the second reaction of Equation (1) was done by Bodenstein and Ramstetter (6) using a furnace heated reaction vessel in the temperature range 592 to 656 °K. Similar experiments were carried out by Rosser and Wise (7) in the temperature range 630 to 1020 °K, and by Ashmore and Burnett (9) in the temperature range 473 to 707 °K. Huffman and Davidson (8) also investigated this reaction in a shock tube in the temperature range 1400 to 2300 °K. Our work covered a temperature range of 1300 to 2100 °K. The results of all these efforts indicated that the reaction mechanism for this reaction was not as straightforward as for the first reaction. Bodenstein and Ramstetter (6), and Rosser and Wise (7) suggested a simple bimolecular reaction,

$$\left(\frac{\partial [NO_2]}{\partial t}\right)_T = - k_{D2b} [NO_2]^2 \tag{65}$$

where the value $k_{D2b} = 4.0 \times 10^9 \exp(-26{,}900/RT)$ ℓ/mole-sec was obtained. Ashmore and Burnett (9) observed a faster initial rate of dissociation than the previous two investigators. But as the reaction proceeded and NO was produced they achieved a similar result. The anomalously fast rate was ascribed to the additional following mechanisms:

$$2NO_2 \underset{k_3}{\overset{k_2}{\rightleftharpoons}} NO_3 + NO \tag{66}$$

and

$$NO_3 + NO_2 \xrightarrow{k_4} NO_2 + NO + O_2 \tag{67}$$

Huffman and Davidson (8) proposed the result

$$\left(\frac{\partial [NO_2]}{\partial t}\right)_T = - k_{D2b} [NO_2]^2 - k_{D2u} [NO_2][M] \tag{68}$$

in which the second term is important at high temperatures and low NO_2 concentrations. Values of the rate constants of $k_{D2b} = 2.5 \times 10^{10} \exp(-25{,}000/RT)$ ℓ/mole-sec and $k_{D2u} = 3.06 \times 10^{13} \exp(-65{,}400/RT)$ ℓ/mole-sec were proposed. This value of k_{D2b} is eight times higher than the previous values, however, no explanation of the discrepancy was given. In this work, a rate equation of the form of Equation (68) was assumed, but somewhat different values of the rate constants were obtained than those of

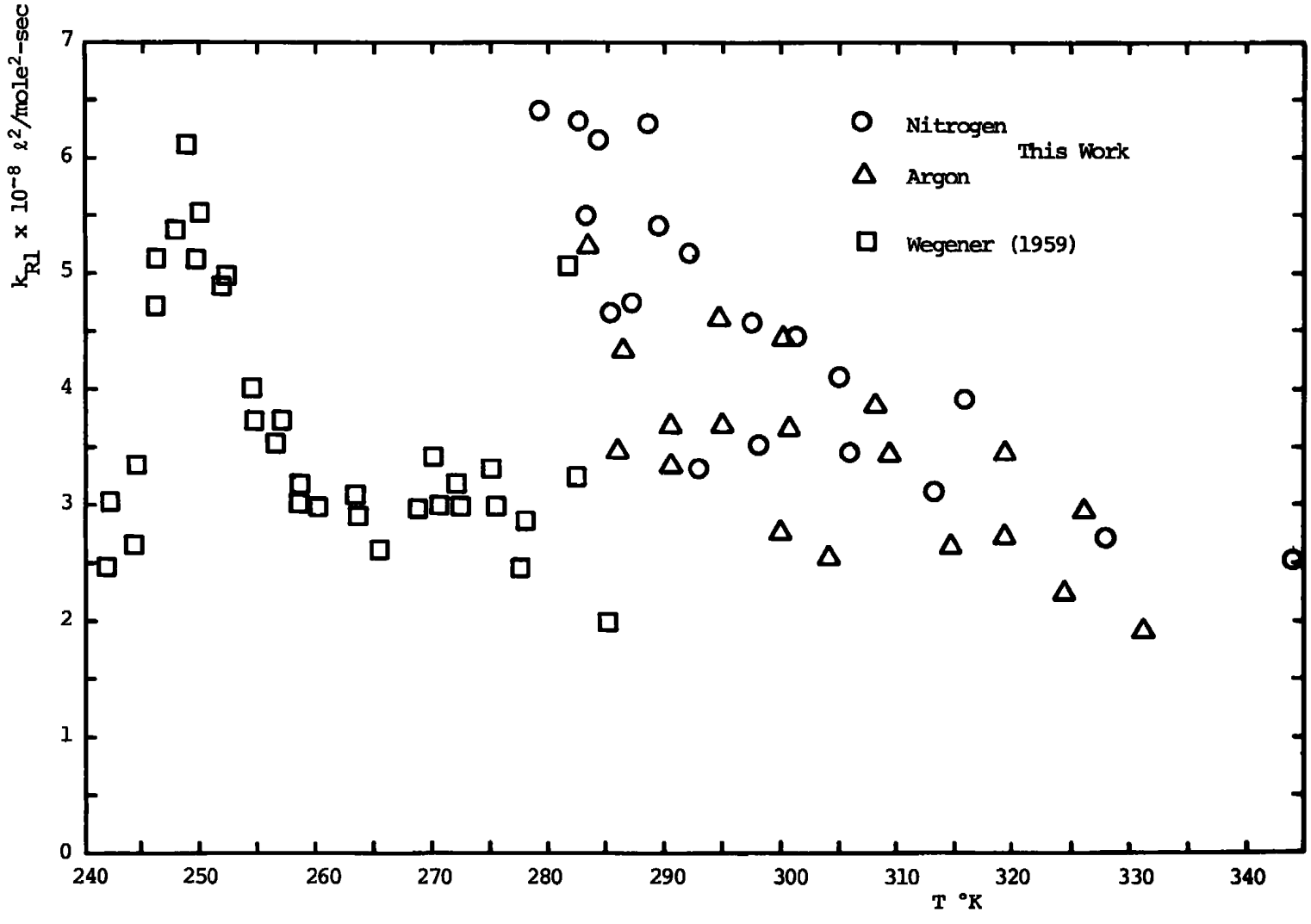

Fig. 9 Recombination Rate Constant versus Temperature

AEDC-TR-69-229

Huffman and Davidson (8).

In Equation (68) both terms on the right hand side are of second order. Following Huffman and Davidson (8) they may also be denoted as the bimolecular and the unimolecular dissociation terms respectively. For the high temperatures observed for this reaction, the effect of recombination was negligible and it could be neglected.

Figure 10 includes a plot of k_{D2b} vs. $1/T$ determined from our experiments by assuming a rate equation of the form proposed by Rosser and Wise (7), Equation (65). It is seen that these points approach the values of Rosser and Wise shown by a curve at the low temperature end of the scale (large values of $1/T$), but they are much too large for higher temperatures.

The experimental constant, in expressions for the rate constants such as (63) and (64), refers to the activation energy for a specific reaction. Accordingly, the results of Rosser and Wise (7) corresponds to the activation energy of the bimolecular reaction. Since the points of Figure 10 indicate a much larger value of the activation energy at high temperatures (i.e., an increased value of the slope) a second reaction was considered corresponding to a higher value of the activation energy. This second reaction path would dominate the bimolecular reaction at high temperatures, but would be insignificant in the temperature range considered by Rosser and Wise (7).

We note that in Figure 10 and in Figure 11, the solid lines represent the values of the rate constants arrived at by a trial and error procedure discussed later. It is also noted that the points in Figures 10 and 11 serve to indicate the form of the rate equation rather than to give values of the rate constants.

Following Huffman and Davidson, the mechanism for a unimolecular reaction was examined suggesting,

$$NO_2 + M \xrightarrow{k_{D2u}} NO + O + M \tag{69}$$

and

$$O + NO_2 \xrightarrow{k_5} O_2 + NO \text{ (fast)} \tag{70}$$

Reaction (69) gives the unimolecular dissociation mechanism while reaction (70) is sufficiently fast ($\tau < 8$ μs) to be considered in equilibrium (8). Accordingly, the rate equation for reaction (69) is proposed to be,

$$\left(\frac{\partial [NO_2]}{\partial t}\right)_T = - k_{D2u} [NO_2][M] \tag{71}$$

where M is any particle participating in the reaction. Using this equation,

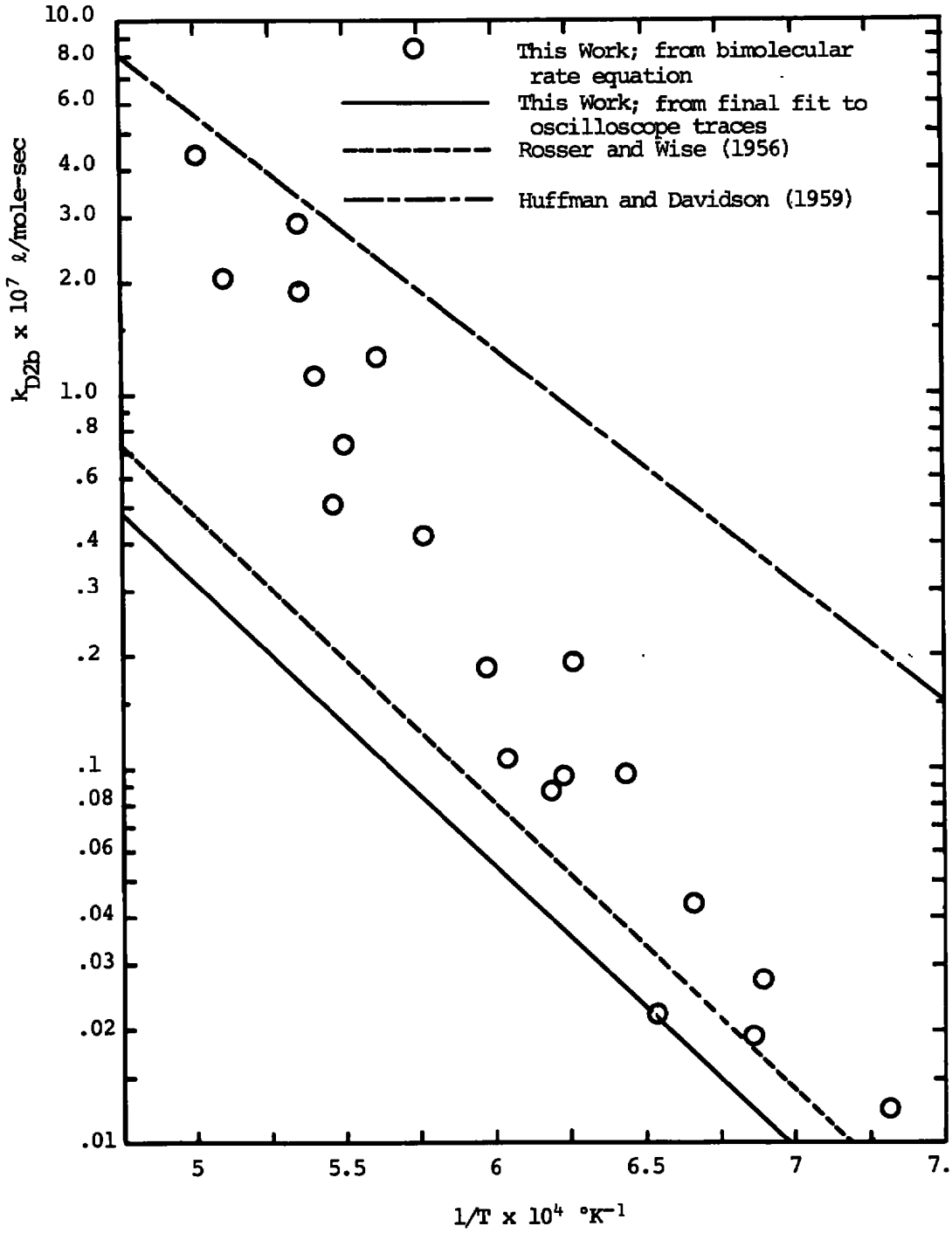

Fig. 10 Bimolecular Rate Constant versus 1/T for

$$k_{D2b} = -\frac{1}{[NO_2]^2}\frac{d[NO_2]}{dt}$$

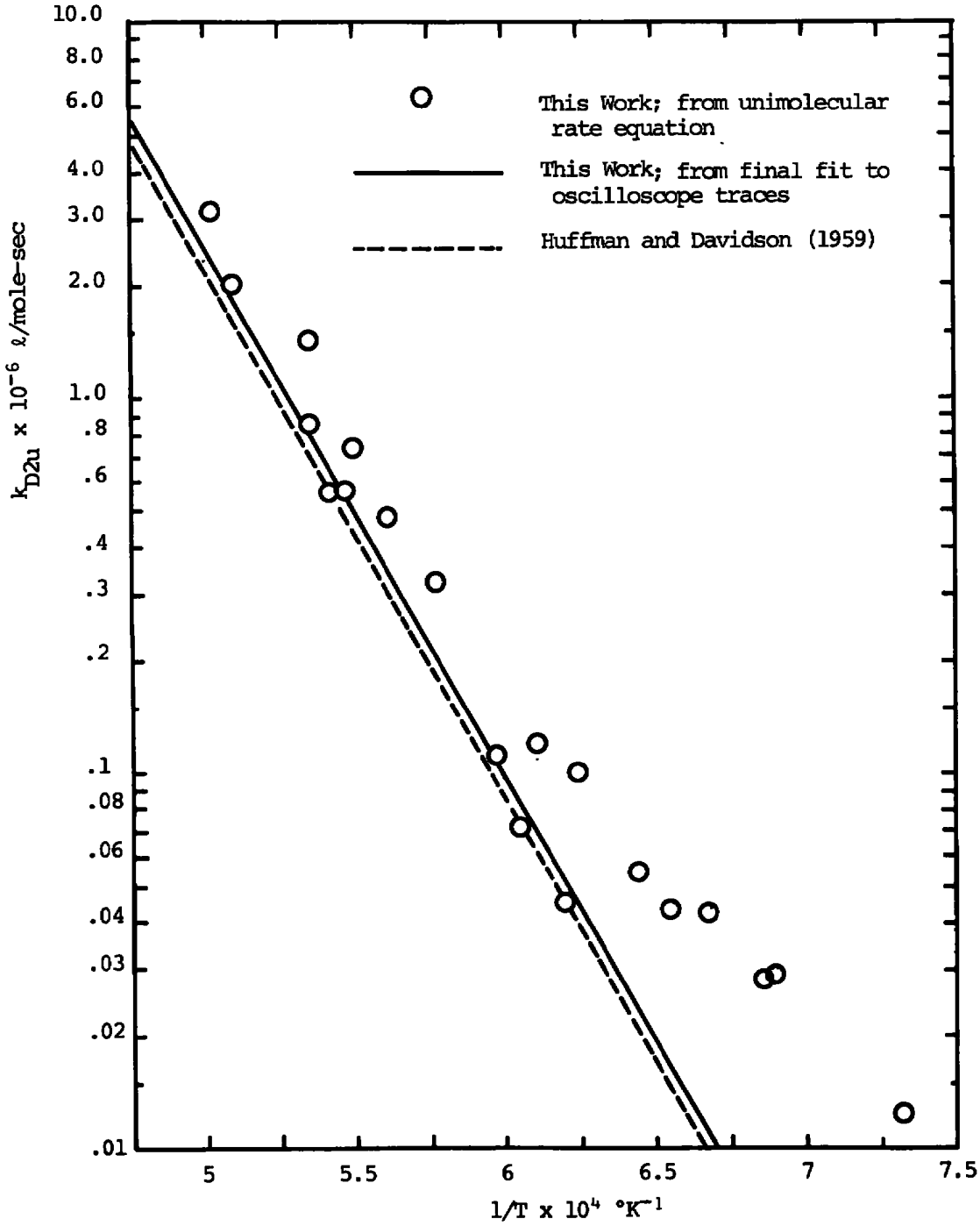

Fig. 11 Unimolecular Rate Constant versus 1/T for

$$k_{D2u} = - \frac{1}{[M]\ [NO_2]} \frac{d[NO_2]}{dt}$$

the results of Figure 10 were recompiled and they are shown in Figure 11. Here, the slope of the line drawn through the high temperature points corresponds to the activation energy predicted for the unimolecular process. The experimental points therefore suggest that the rate equation for the complete reaction is indeed that of Equation (68).

As mentioned, the rate constants themselves were arrived at by using a trial and error procedure. Initial values of the rate constants were chosen as the assymptotes of the two sets of points in Figures 10 and 11. Using the theory presented in Section III, the theoretical NO_2 concentration was calculated as a function of t_{lab}. These values were then compared directly with the experimental traces of Figure 6. The rate constants were then adjusted until the calculated results fit the experimental traces for both high and low temperature experiments. The details of this technique are presented in Section VII. The rate constants thus derived were,

$$k_{D2b} = 3.0 \times 10^{9} \exp(-26{,}900/RT) \text{ ℓ/mole-sec} \quad (72)$$

and

$$k_{D2u} = 3.60 \times 10^{13} \exp(-65{,}400/RT) \text{ ℓ/mole-sec} \quad (73)$$

These are plotted as the solid lines in Figures 10 and 11 respectively. These values are in agreement with those of Rosser and Wise (7) for the low temperature limit, and with those of Huffman and Davidson (8) for the high temperature limit.

SECTION VII
NON-EQUILIBRIUM FLOW FIELDS WITH CHEMICAL REACTIONS

When the values of the rate constants are known together with the appropriate rate equations, the methods of Section III can be employed to solve the conservation equations for the time dependent variables of state. The resulting set of eight simultaneous non-linear first order differential equations may be solved numerically. With these results, Equation (38) provides the NO_2 concentration which can be plotted vs. the distance downstream of the shock front. The experimental traces and Equation (39) similarly can provide a plot of $[NO_2]$ vs. x where $x = U_1 t_{lab}$.

Figures 12, 13 and 14 give the NO_2 concentration normalized by the NO_2 concentration at state 1 as a function of distance x for the nine experiments shown previously in Figure 5. Argon was present as the inert gas. The experiments shown are for shock strengths applicable to the first reaction of Equation (1) only. The chief source of error in obtaining the rate constants from the oscilloscope traces is incurred in the measurements of slope of the photomultiplier signal with a certain amount of electronic noise present. Figures 12, 13 and 14 serve as a check on the validity of the rate constant measurements, and they help to eliminate the uncertainty of the slope measurements. Not only do these graphs corroborate the values of the rate constants, but they justify the analytical methods of Section III. Figures 13 and 14 demonstrate that the calculated conditions after the normal shock jump are within a few percent of the experimental values. Similarly, the conditions for final equilibrium are in good agreement.

Figure 12 shows the conditions for three fully dispersed shock waves of different strengths. The fit between theoretical and experimental values is excellent, demonstrating why the use of these waves is ideal for a study of chemical kinetics as suggested in Section I. Similarly, Figures 13 and 14 show the experimental vs. the theoretical NO_2 concentration ratio for six partly dispersed waves. The agreement is again seen to be good. In experiment 496 though, the experimental points fall slightly below the theoretical curve. This is due to the fact that the limit of resolution of the equipment is being reached and there appears to be an electronic lag in the signal.

Figures 15, 16, and 17 show the calculated properties of α , β , p/p_1 , T/T_1 , and U/U_1 vs. time in the shock fixed coordinate system. For these experiments the solutions were integrated from the appropriate equations from the initial conditions of $t = 0$ at the shock front to $t = \tau_\alpha$ where τ_α is defined in Equation (37). The initial properties for these graphs are given in Table II.1.

Figure 15 shows the continuous change in state variables for a fully dispersed wave. Figures 16 and 17 show the change of variables after the normal shock front at $t = 0$. The behavior of the temperature ratio is of interest in that it first rises and then falls to its final value. This is due to the energy added by the convective motion of the slowing gas flow as

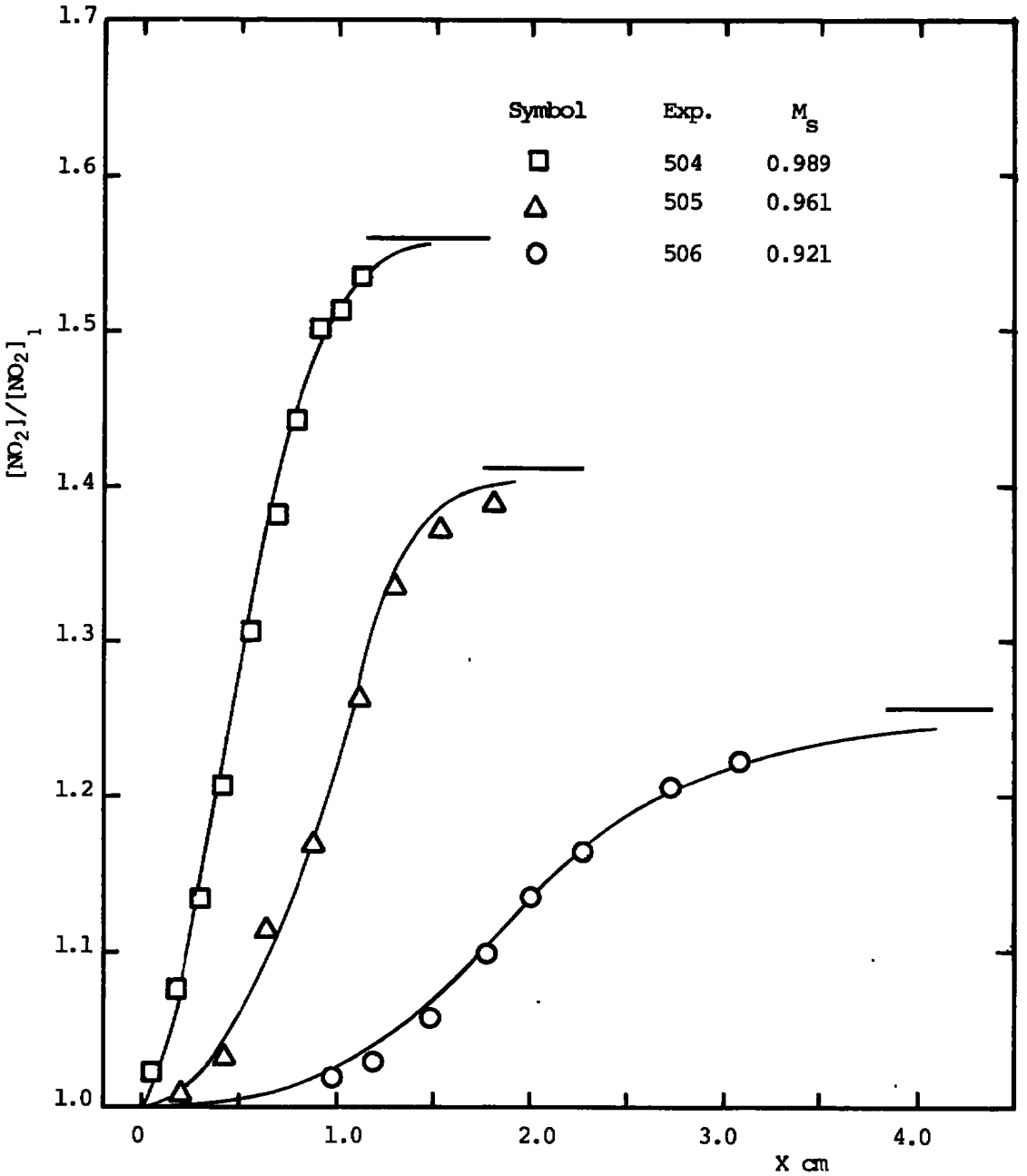

Fig. 12 Theoretical and Experimental NO_2 Concentration Ratios versus Distance for Fully Dispersed Shock Waves

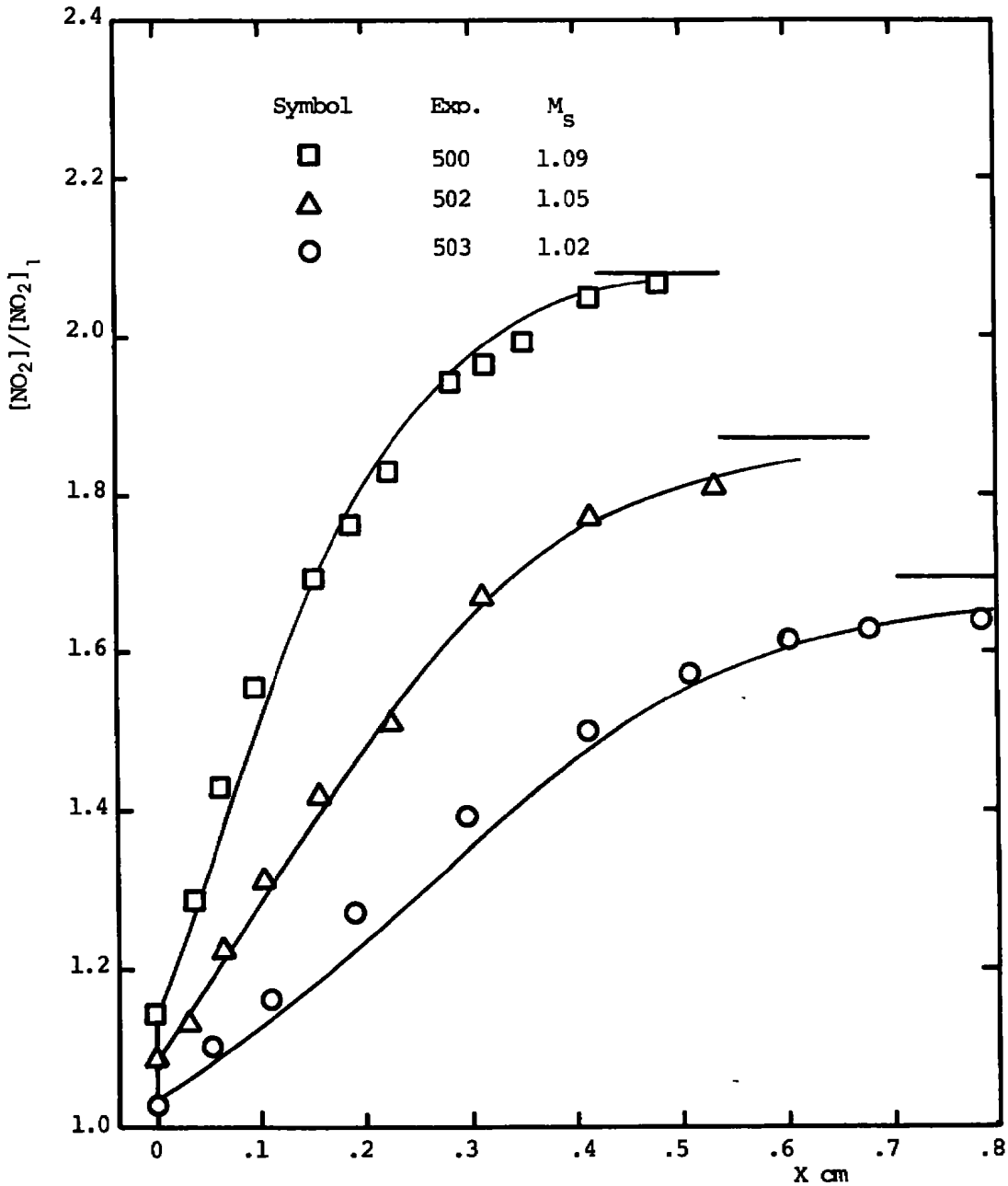

$[NO_2]_1 = 0.827 \times 10^{-3}$ moles/liter $P_1 = 200$ Torr $T_1 = 280.6$ °K

$X_o = 0.0793$

Fig. 13 Theoretical and Experimental NO_2 Concentration Ratios versus Distance for Weak Partly Dispersed Waves

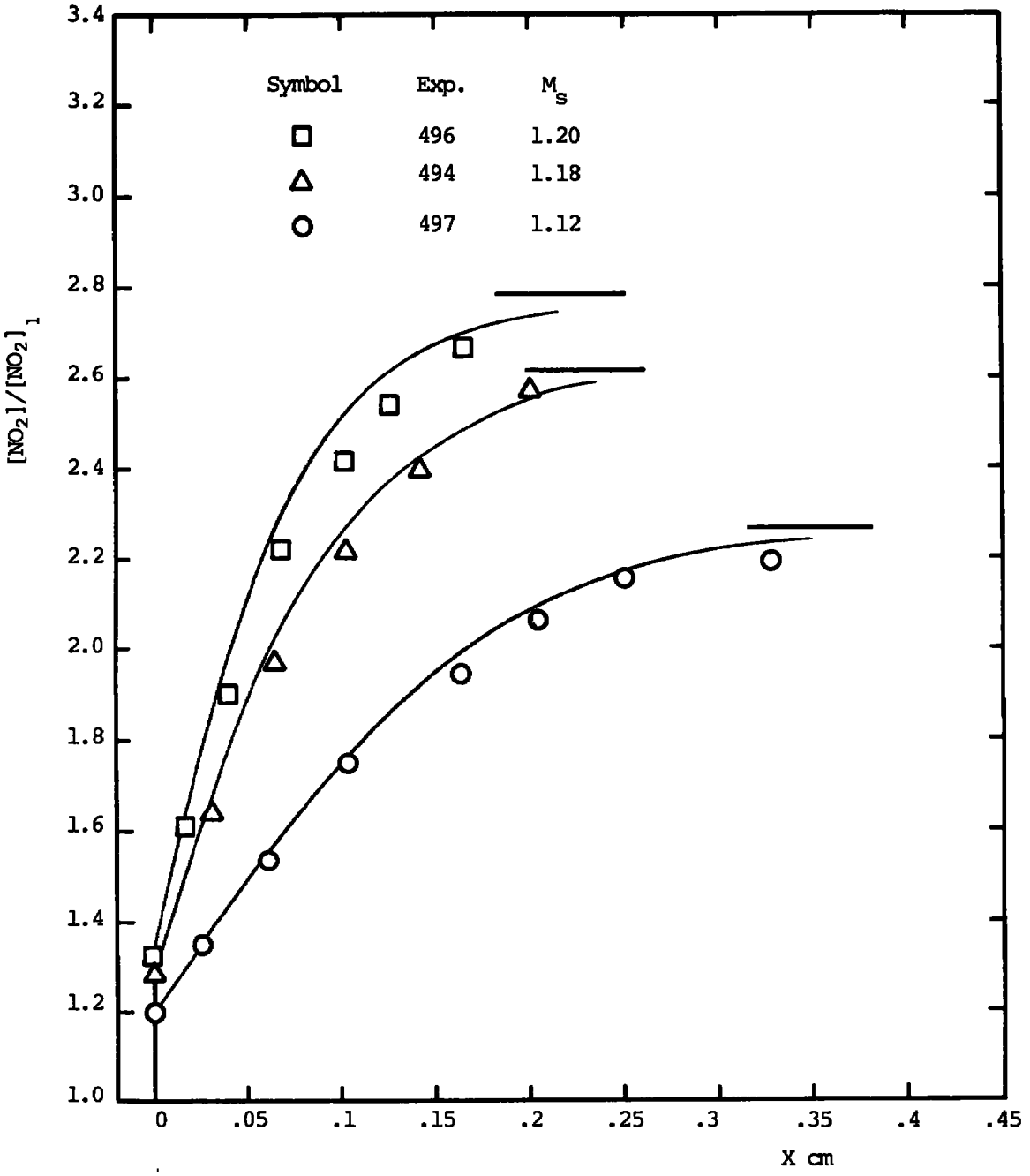

Fig. 14 Theoretical and Experimental NO_2 Concentration Ratios versus Distance for Partly Dispersed Shock Waves

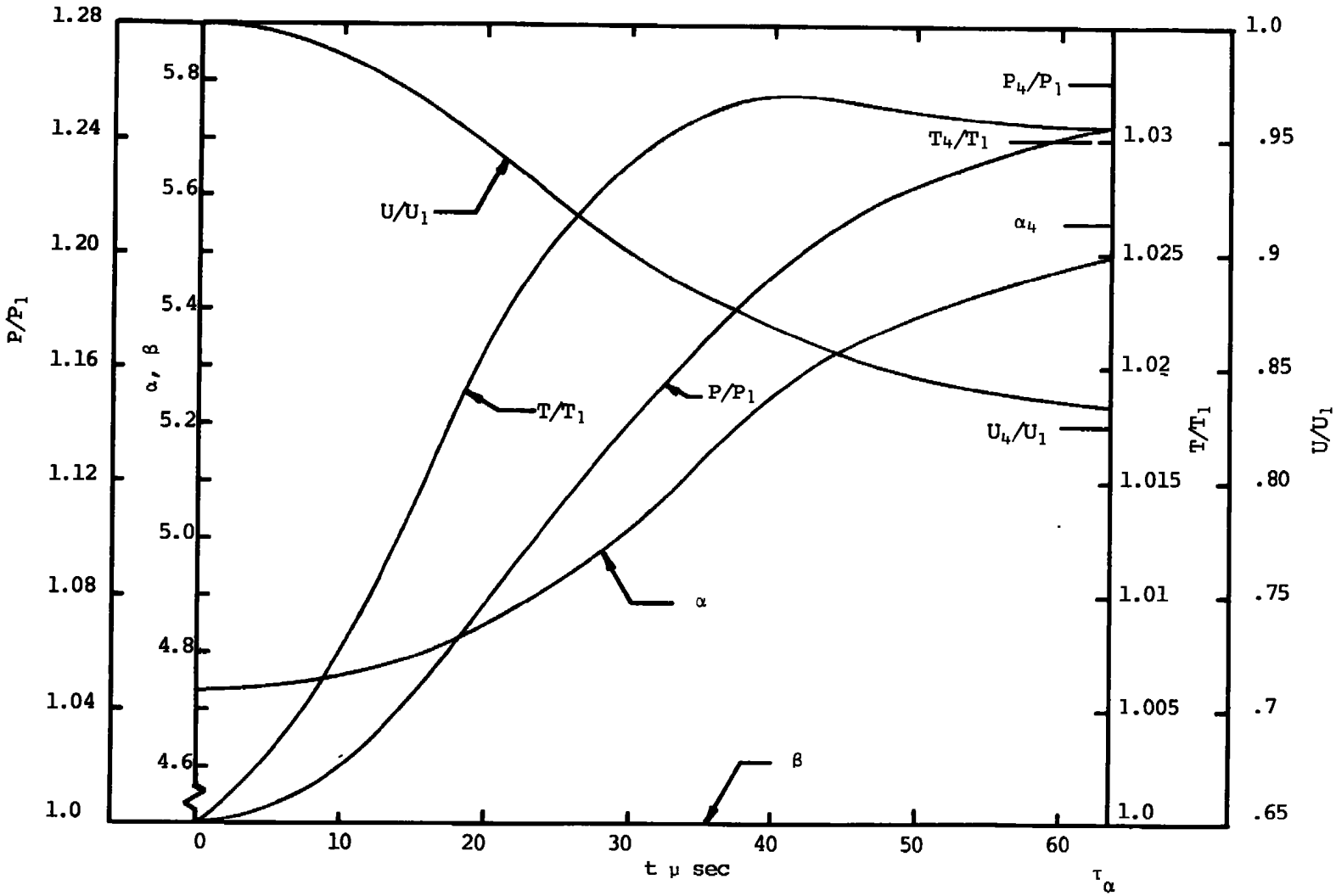

Fig. 15 Calculated Conditions behind Shock Front (Exp. 505, M_s = 0.961)

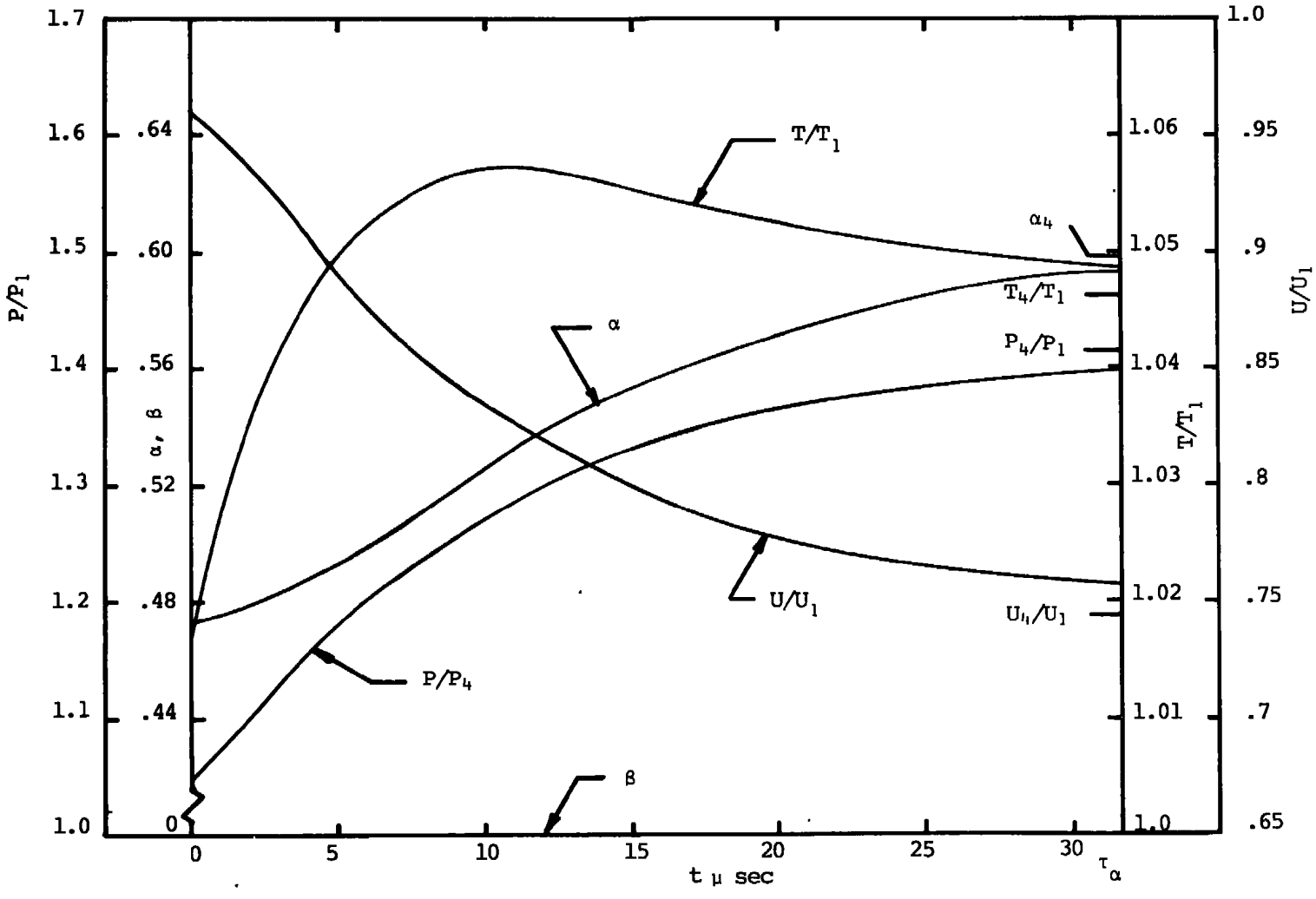

Fig. 16 Calculated Conditions behind Shock Front (exp. 503, M_s = 1.02)

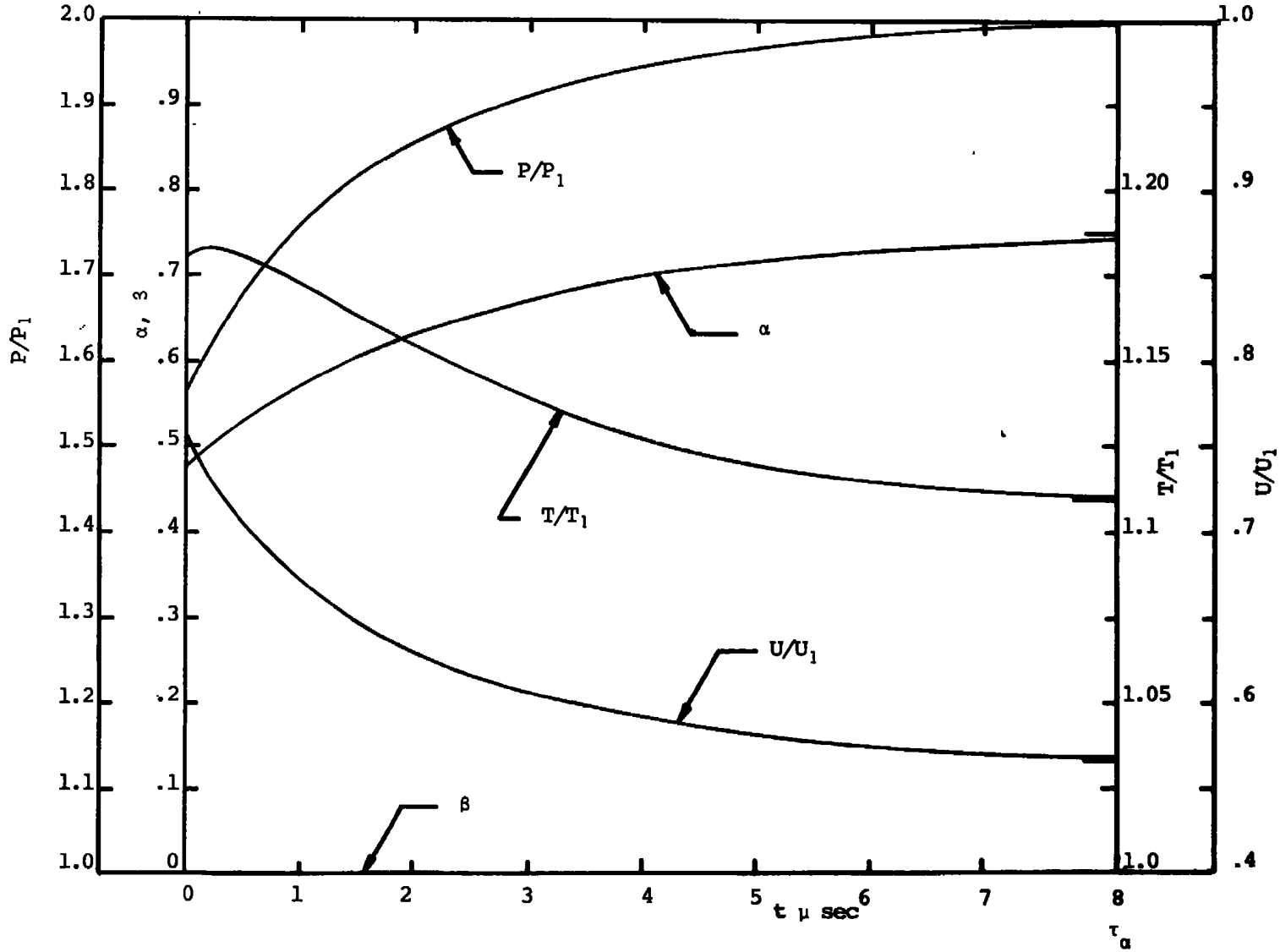

Fig. 17 Calculated Conditions behind Shock Front (Exp. 496, M_s = 1.21)

opposed to the energy subtracted by the endothermic chemical reaction. For sufficiently strong shocks, the endothermic reaction dominates and the temperature decreases monotonically.

A flow field with more than one non-equilibrium mode may be experimentally investigated by one of several methods. If the relaxation times for these degrees of freedom are of the same order of magnitude, and the reactions occur in the same temperature interval, then it is necessary to measure a time dependent variable of state for each non-equilibrium mode. For example, in a chemical relaxing flow with two simultaneous reactions it would be necessary to concurrently measure two state variables such as the concentrations of two species of the reaction. In this work, we have the advantage that the two reactions can be uncoupled since $\tau_\beta >> \tau_\alpha$, and it was only necessary to measure one progress variable i.e. the time dependent NO_2 concentration. Because of the large temperature changes introduced by strong shock waves, it was found necessary as described to account for the temperature dependence of the extinction coefficient ε in Equation (39). Due to this it was necessary to measure the rate constants and the extinction coefficient simultaneously. An iterative procedure was employed in which values of the rate constants were assumed and adjusted by comparing the calculated and experimental values of the time dependent NO_2 concentrations. Finally, the calculated conditions at state 3 and Equation (39) were used to obtain the values of $\varepsilon(T)$ shown in Figure 4.

Figure 18 shows the theoretical and experimental NO_2 concentration ratios for four experiments utilizing the values of Equations (42), (64), (72), and (73). At state 3, values of $[NO_2]_{\beta 3}/[NO_2]_1$ were calculated assuming that the second reaction is frozen while the first reaction goes to equilibrium. Since the initial rate of dissociation of NO_2 is fairly rapid the maximum value of $[NO_2]_3/[NO_2]_1$ obtained, as computed kinetically, is less than the frozen value (Figure 18). Therefore, state 3 was defined as the actual conditions at which the first reaction goes practically to equilibrium. This state corresponded to the maximum NO_2 concentration. Since the first reaction reached equilibrium within 0.1 μs, the assumption that state 3 exists immediately following the normal shock jump was justified. In calculating conditions at state 3, the Ashmore and Burnett (9) reaction mechanisms of Equations (66) and (67) were not considered. This was justified since the mechanism of Equation (69) dominates the reaction at high temperatures. In Table II.2 a comparison of the values at state 3 for β either frozen or relaxed is given. Finally, Figure 19 shows several calculated properties for experiment 599.

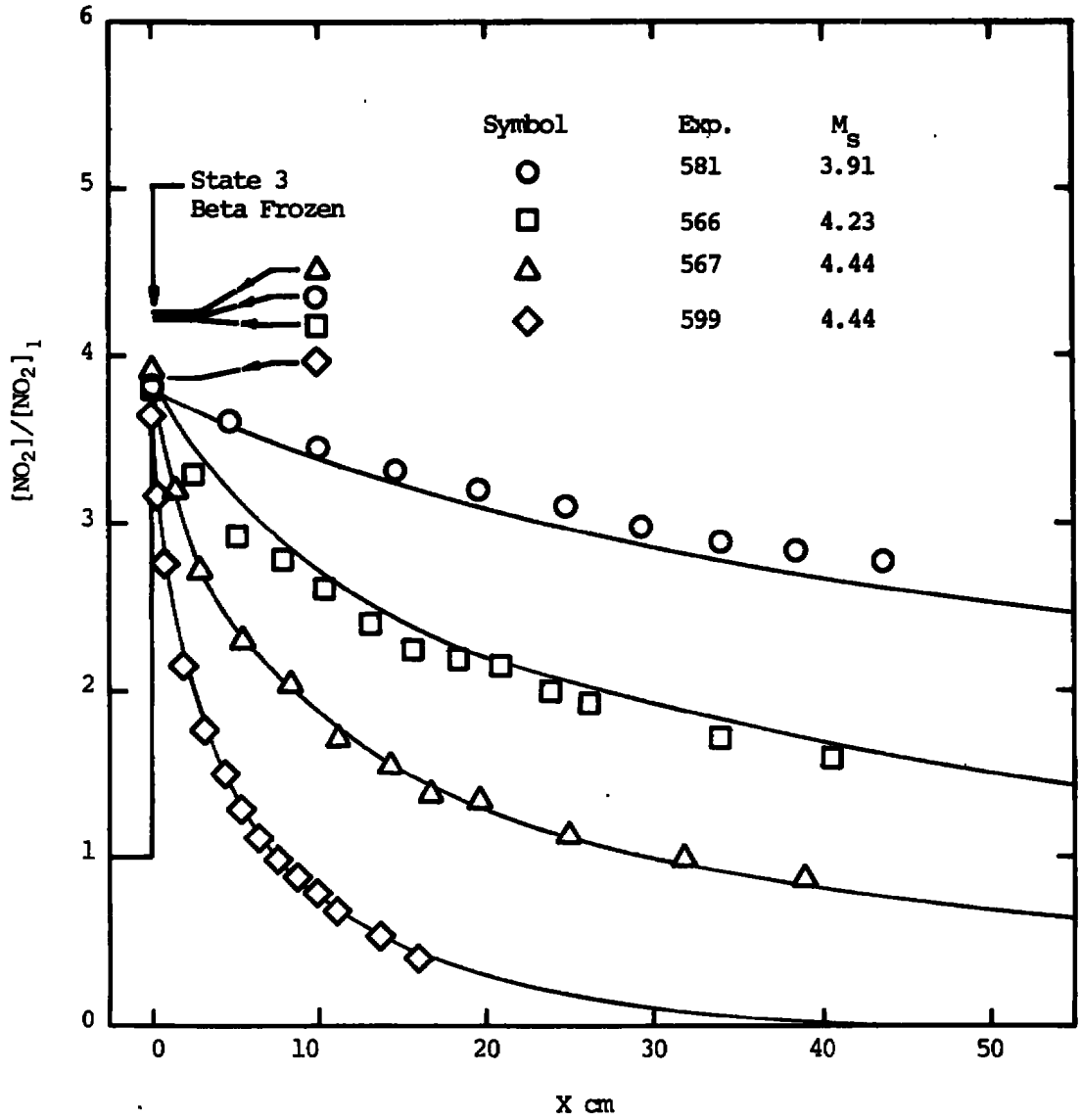

Fig. 18 Theoretical and Experimental NO_2 Concentration Ratios versus Distance for Strong Partly Dispersed Shock Waves. Conditions Given after Normal Shock for Beta Frozen and Relaxed

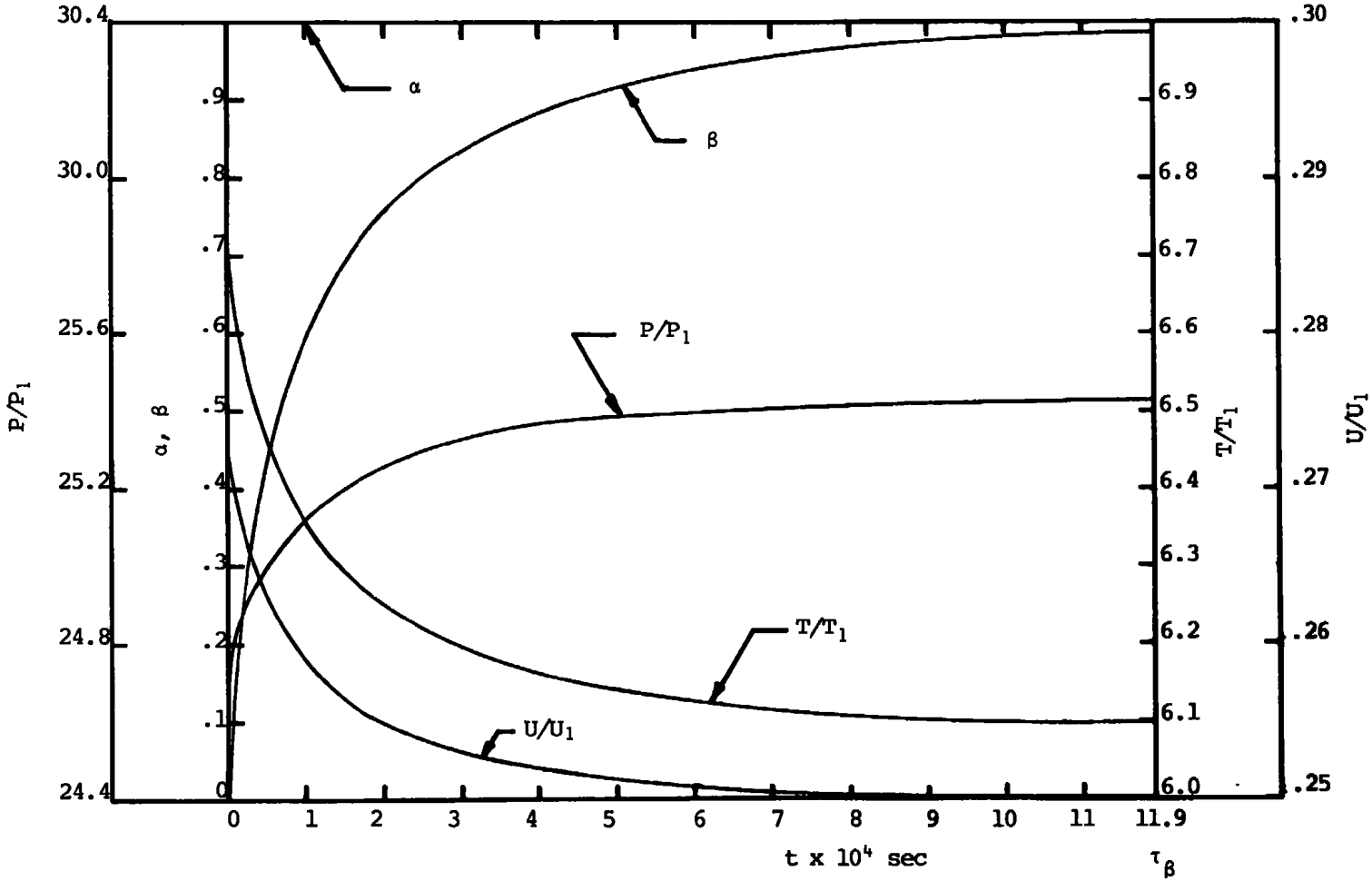

Fig. 19 Calculated Conditions behind Shock Front (Exp. 599, M_s = 4.44)

SECTION VIII
SUMMARY

This work is concerned with the non-equilibrium flow of a chemically reacting gas mixture through a shock wave in a shock tube. Two chemical reactions: $N_2O_4 + M \rightleftarrows 2NO_2 + M \rightleftarrows 2NO + O_2 + M$, were observed utilizing a light absorption technique permitting the time dependent concentration of the species NO_2 to be determined. Argon and nitrogen were used as the inert carrier gas M. The second of the two reactions studied has a relaxation time several orders of magnitude larger than the first reaction and moreover it takes place at higher temperatures. This allowed the two reactions to be experimentally uncoupled. In turn, both chemical relaxation times were large compared to the translational, rotational and vibrational relaxation times. Therefore, all molecular degrees of freedom other than those pertaining to the chemical reactions could be considered in equilibrium throughout the flow field.

One aim of this work was the investigation of the passage of shock waves in a shock tube through a gas mixture in which only one non-equilibrium degree of freedom was excited, i.e., the first of the above chemical reactions. The interplay between the normal shock jump and the chemical relaxation zone was examined as a function of shock strengths. This produced a complete picture of the flow field as the shock strengths were varied from weak fully dispersed waves, (propagating below the frozen sound speed), to the stronger partly dispersed waves, (propagating above the frozen sound speed). Fully dispersed waves in a chemically reacting system were observed for the first time and these waves were found to be ideally suited for chemical kinetic studies due to the inherently long relaxation lengths and small gradients in the state variables.

For stronger shock strengths, the second reaction was observed where the two reactions were uncoupled due to the large difference in their respective relaxation times. Utilizing this technique, a composite picture of a flow field with two non-equilibrium degrees of freedom was formed. Because these two reactions could be examined independently, it was only necessary to measure one time dependent variable of state, the NO_2 concentration, in order to describe the flow field.

Finally, a study of the reaction mechanisms and rate constants for both reactions was carried out. For the first reaction, following Wegener (2) the rate equation was taken to be $d[N_2O_4]/dt = - k_{D1} [N_2O_4][M] + k_{R1} [NO_2]^2[M]$. For argon as the inert gas, the rate constant was found to be $k_{D1} = 2.23 \times 10^{14} \exp (- 11000/RT)$ ℓ mole^{-1} sec^{-1} where k_{R1} is related to k_{D1} by the equilibrium constant. This value was in good agreement with the values of other investigators. For the second reaction, following Huffman and Davidson (8) the rate equation was taken to be $d[NO_2]/dt = - k_{D2b} [NO_2]^2 - k_{D2u} [NO_2][M]$. For argon again taken as the inert gas the two dissociation rate constants were found to be $k_{D2b} = 3.0 \times 10^9 \exp (- 26900/RT)$ ℓ mole^{-1} sec^{-1} and $k_{D2u} = 3.60 \times 10^{13} \exp (- 65400/RT)$ ℓ mole^{-1} sec^{-1}. The first term was found to be important for temperatures below 1200 °K while

the second term became dominant for higher temperatures.

An analytical description of the flow fields was performed with the assumptions made that effects of viscosity, heat conduction, and diffusion, were negligible outside the classical shock region. Also, the species of the gas mixture were individually considered to be thermally perfect. The steady state conservation equations were then solved numerically together with the equations of state and the two appropriate rate equations. This determined the time dependent histories of the state variables in the flow. The NO_2 concentrations calculated in this fashion agreed well with the experimental values determined by the light absorption technique.

By observing the behavior of a particular well known set of chemical reactions in a flow with shock waves of varying strength the generalized behavior of a non-equilibrium flow field with shock waves was evidenced.

APPENDIX I
DESCRIPTION OF EQUIPMENT

Figures I.1 and I.2 are a sketch and a photograph respectively of the shock tube, chemical mixing station, and instrumentation. The overall length of the shock tube is 26 feet 8 inches and the tube is constructed of seamless stainless steel 304 tubing. The I.D. of the tube is 3.020 inches and the O.D. is 3.25 inches, except for the test section whose O.D. is 3.50 inches. The driven tube is divided into three sections as shown. These sections are bolted together across 1 inch inserts which hold teflon "O" rings. The inside of the tube was honed to insure a uniform cross-section and smooth walls. Around each length of the driven tube, a concentric 4 inch steel pipe has been welded, forming a jacket which may be cooled or heated by an appropriate fluid. A foam rubber insulation covers the jacket and the manifold connected to the jacket. Fourteen copper-constantan thermocouples at 20 inch intervals are inserted in the jacket to monitor the tube temperature. At the end wall a thermocouple is inserted directly into the tube to measure the gas temperature.

Flats were milled on the test section for three sets of 0.5 inch thick quartz windows. The flats reduce the wall thickness of the tube at the windows to 1/32 inch so that the windows lie fairly flush with the inside diameter. The spacing between the windows was measured to be 8.136 cm, and this is the optical length used in the absorption measurements. The two outer pairs of windows are used for the passage of light beams acting as trigger stations for timing the shock speed and initiating the scope trigger. They are 1.00 meters apart. The center windows are used for the light absorption station.

The 4 foot driver section is mounted on rollers so that the tube may be easily opened to insert the diaphragms. (For certain experiments, a six foot driver section was used). The driver section is attached to the rest of the tube by fast acting clamps. A housing is welded on the driver section containing a spring loaded firing pin used to rupture the diaphragms. The entire shock tube is rigidly mounted on a welded frame of 4 inch I beam and 4 inch pipe. The frame is bolted to the floor of the laboratory.

The driver and driven sections are connected to the chemical mixing station and to vacuum pumps by 0.5 inch O.D. stainless steel tubing. The driver section is independent of the driven section so that it may be evacuated and filled simultaneously with the driven section. The system may be connected to one of the two vacuum pumps, a Nash-Hitor roughing pump or a Welsh Duo-seal floor pump. By attaching a diffusion pump with a cold trap the system could be pumped down to 10 microns. The outer two windows of the test section as shown in Figure I.1 are used for shock detection. As described by Eberstein (37) an optical triggering system was found advisable for the weak shocks and relatively high pressures (above 30 torr) of interest. The detection system may be used in one of two configurations. The first configuration is a standard schlieren deflection system. A narrow slightly converging beam of light is focused just outside a 0.125 inch diameter fiber

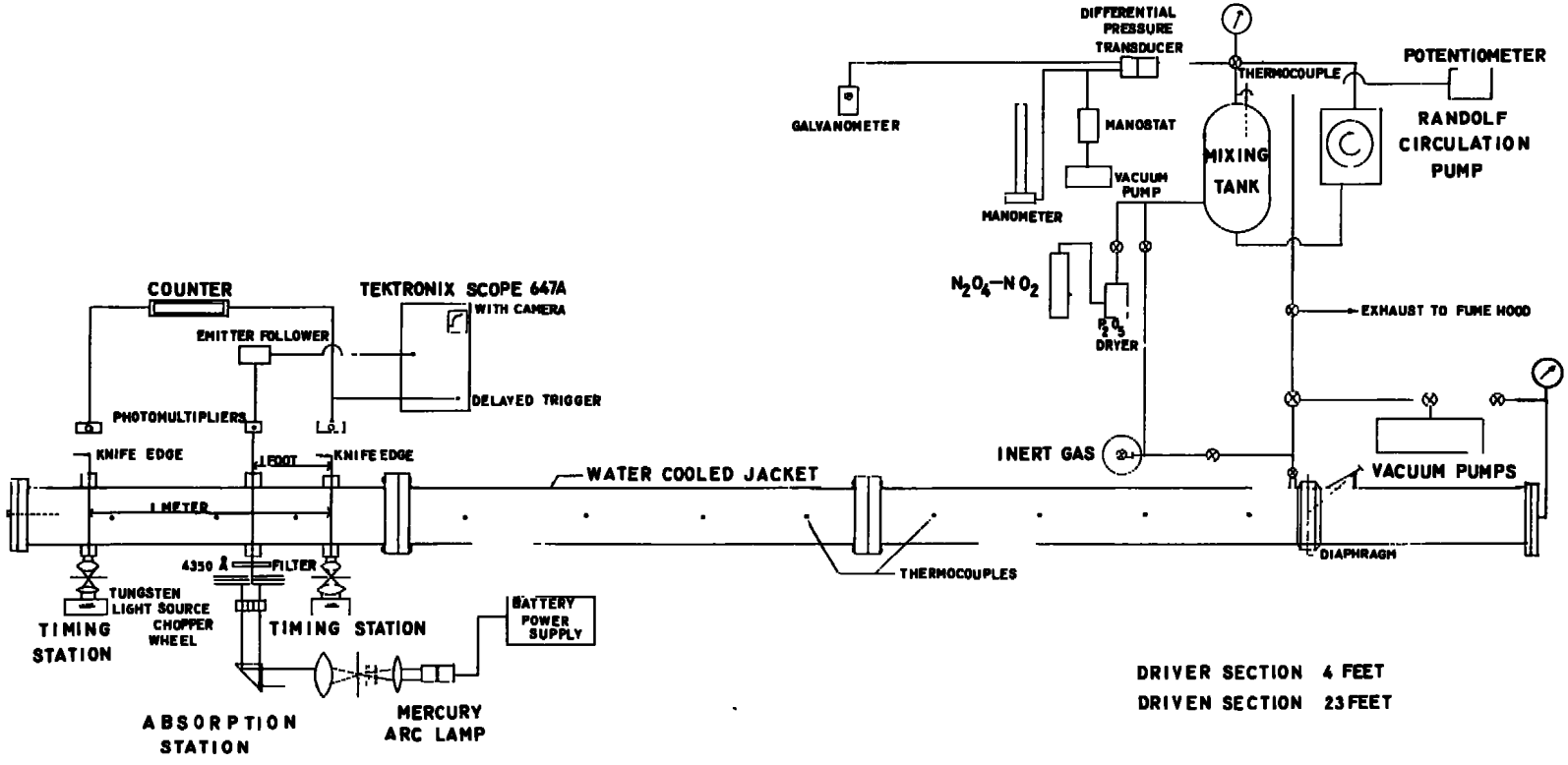

Fig. I-1 3-in.-ID Cooled Shock Tube and Gas Mixing Station

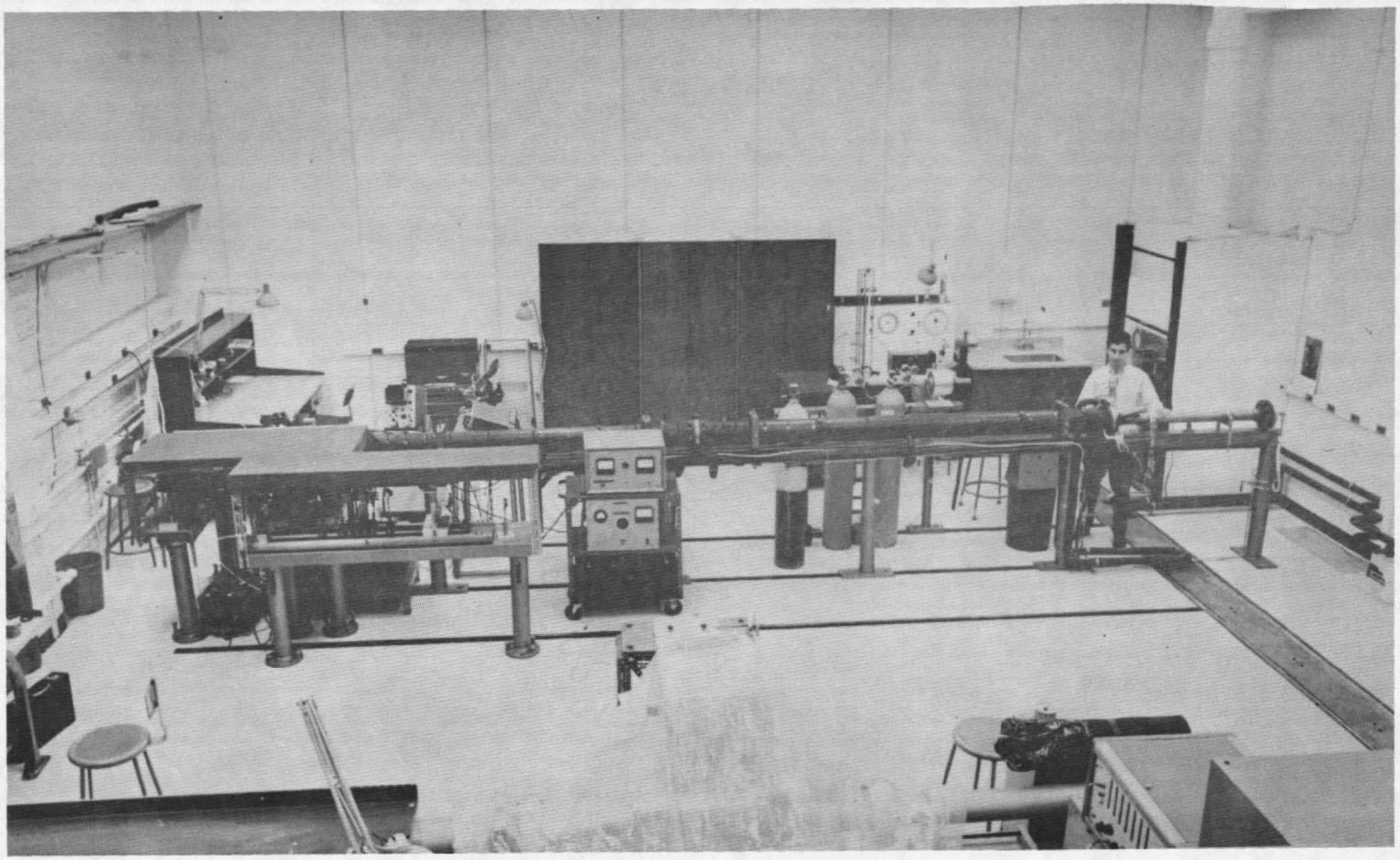

Fig. I-2 Photograph of Shock Tube and Gas Mixing Systems

optic light guide. The light guide leads to a RCA 931 A photomultiplier tube. The density change across the shock deflects the beam into the light guide and the resulting signal is fed into a pulse amplifier giving a response time to the shock of less than 0.5 μs. This technique was not successful for the extremely weak fully dispersed shocks and at pressures below 80 mm Hg for shocks of moderate strength. A trigger system dependent on the absorptive properties of NO_2 was developed for these situations. In this configuration, a 4350 Å filter is placed in the light beam, and the beam is focused directly on the fiber optic light guide. Since NO_2 strongly absorbs light at this wave length, the increase in density of NO_2 through the shock causes a sharp decrease in signal. This method of triggering was successful for all shock strengths and pressures used. The signal from the first trigger station was used to start the type 5233L Hewlett Packard Electronic Counter and to trigger the delay unit in the oscilloscope. The other station 1 meter downstream stopped the counter giving the shock speed. The absorption station as shown in Figure I.1 consists of a narrow parallel monochromatic beam of light passing through the shock tube at right angles to the direction of fluid flow and impinging on a photomultiplier tube. The light source used was a PEK high pressure mercury arc lamp type 107 with a storage battery power supply to insure a steady DC light signal. The light was collimated by a series of slits to produce a parallel beam. The light was then passed through a Bausch and Lomb 4350 Å absorption filter with a half width of 50 Å. After passage through the tube, the light entered a RCA IP21 photomultiplier tube powered by a Hamner high voltage power supply type N401. An emitter-follower was used to increase the electronic response time and the resulting signal was recorded on a Tektronix type 647A oscilloscope with a built in delay unit, and a Polaroid camera attachment.

A high speed chopper wheel may be placed in the light path and it is used for calibration purposes prior to a run. The chopper is run by an air driven drill turbine and it is capable of chopping at a rate of 20 Khz. Besides being used to measure the incident DC light signal, the chopper is used in conjunction with measurements to measure either the electronic response time or the slit width. Since the measured rise time is a combination of electronic response and the time necessary for the chopper blade to pass through the light beam, by measuring the rise time of the signal for a known chopping rate the electronic rise time was computed for a known slit width. The electronic rise time was of the order of 0.5 μs which was sufficiently fast compared to the chemical processes studied. Calibrated neutral density filters may also be placed in the light path to measure the linearity of the photomultiplier, and to control the light input.

The mixing system, as shown in Figure I.1 consists of a tank of volume 34.4 liters, a circulating pump, and a system of valves to admit gases to the tank, connect vacuum pumps to the tank, and allow the gas mixture in the tanks to flow into the shock tube. Due to the poisonous and corrosive nature of the gases used, the components of the mixing station were constructed of stainless steel and teflon, and it was placed in a walk-in type fume hood. The temperature in the tank was measured with a copper-constantan thermocouple, and the pressure was measured roughly with a bourdon type gage and more accurately with a differential stainless steel diaphragm strain gage pressure transducer (Dynisco model DPT 85-2). The transducer

acts as a null gage in which the pressure in the tanks was balanced by a manostat and the pressure was read on a Wallace and Tiernan type FA 187 mercury manometer or on a Wallace and Tiernan pressure gage model FA 145 to an accuracy of 0.1 torr. This technique was necessary since the reacting gas attacks mercury.

In practice, the mixing tank was evacuated to less than 1 torr and flushed with the inert gas to be used in the mixture. The procedure was repeated twice. The tank was then filled to a pressure of about 100 torr with the inert gas. The N_2O_4 - NO_2 was then admitted to achieve the desired mole fraction. Inert gas was then added to a pressure of 2280 torr. At each stage the pressure and temperature were recorded after the system had been allowed to reach equilibrium. The gas mixture was continually circulated through the tank and connecting tubing by means of a Randolf pump. This ensured that the mixture was homogeneous. The gases used were supplied by the Matheson Co. Prepurified nitrogen with a minimum purity of 99.997% by weight and high purity argon of purity 99.995% were used. As a check, research grade argon with a maximum impurity of 1 ppm was used. The N_2O_4 - NO_2 had a minimum purity of 95.5% with the following impurities: water 0.1% max., nitrosyl chloride 0.08% max., nonvolitile (ash) 0.01% max. Additional water vapor was removed by passing the nitrogen dioxide gas through a silica gel drier. To check the purity of the N_2O_4 - NO_2, a series of experiments were performed in which oxygen was allowed to circulate for eight hours through the liquid N_2O_4 in order to oxydize impurities. This procedure did not affect the properties of the gas.

The procedure followed in running the shock tube with a reacting gas mixture was as follows: An N_2O_4 - NO_2 inert gas mixture was prepared as previously discussed. A diaphragm of cellophane or Mylar was placed between the driver and driven sections and the tube was clamped together. Either one or two sheets of diaphragm were used depending upon the pressure ratio. The diaphragm was near its bursting pressure when it ruptured. The shock tube was then evacuated to less than 0.5 torr and was flushed with the inert gas and pumped down again. The reactant gas mixture was next admitted to the tube and its pressure and temperature were measured with the differential pressure transducer and the copper-constantan thermocouple. The driver section was evacuated and the driver gas, argon, nitrogen, or helium was brought up to the required pressure. For very weak shocks, a diaphragm with a bursting pressure of only 250 torr was used. Therefore, care was taken so that this pressure difference was not exceeded when the sections of the tube were being evacuated and filled. The chopper wheel was inserted in the light path and the incident light intensity was calibrated. The chopper wheel was removed from the light path and the shock was initiated by releasing the firing pin. After an experiment, the reactant gas was flushed out of the tube through the fume hood. This was done by filling the tube to 2280 torr with nitrogen and venting it through the hood. This procedure was repeated three times. The tube was then evacuated twice before it was opened to the air. After every few runs a rag soaked in acetone was pulled through the tube to clean it, then a chamois cloth was pulled through to remove any remaining dust or lint.

APPENDIX II
TABULATED VALUES OF THE CALCULATED CONDITIONS ACROSS THE SHOCK WAVE

Tables II.1 and II.2 give the calculated conditions of the flow variables after the normal shock jump (state 2), after the first reaction of Equation (1) has reached equilibrium (state 3), and at the final equilibrium state (state 4). Table II.1 refers to the experiments of Figure 5, and Table II.2 refers to Figure 6.

The initial conditions at state 1 refer to the measured values of p_1 , T_1 , and U_1 from which α_1 , β_1 , and $[NO_2]_1$ are calculated.

In Table II.2, two values are given for conditions after the first reaction has reached equilibrium. The first condition was calculated holding β frozen. The second condition is the value at state 3 with β at its actual value.

TABLE II-1

	Initial Conditions State 1	After Normal Shock State 2	Final Equilibrium State 4
Exp 506	$M_s = 0.921$	$X_o = 0.0793$	
α	0.4735		0.5231
β	0.68×10^{-4}		0.9×10^{-4}
P Torr	200.0		230.6
T °K	280.6		285.7
U m/sec	272.2		241.3
$[NO_2]$ moles/liter	0.827×10^{-3}		0.103×10^{-2}
Exp 505	$M_s = 0.961$	$X_o = 0.0793$	
α	0.4735		0.5551
β	0.68×10^{-4}		0.11×10^{-3}
P Torr	200.0		252.0
T °K	280.6		289.0
U m/sec	283.8		233.4
$[NO_2]$ moles/liter	0.827×10^{-3}		0.118×10^{-2}
Exp 504	$M_s = 0.989$	$X_o = 0.0793$	
α	0.4735		0.5774

TABLE II-1 Continued

	Initial Conditions State 1	After Normal Shock State 2	Final Equilibrium State 4
β	0.68×10^{-4}		0.13×10^{-3}
P Torr	200.0		267.8
T °K	280.6		291.3
U m/sec	292.1		228.4
$[NO_2]$ moles/liter	0.827×10^{-3}		0.129×10^{-2}
Exp 503 $M_s = 1.02$ $X_o = 0.0793$			
α	0.4735	0.4735	0.5980
β	0.68×10^{-4}	0.68×10^{-4}	0.14×10^{-3}
P Torr	200.0	209.2	282.8
T °K	280.6	285.3	293.4
U m/sec	299.9	291.4	223.9
$[NO_2]$ moles/liter	0.827×10^{-3}	0.851×10^{-3}	0.140×10^{-2}
Exp 500 $M_s = 1.09$ $X_o = 0.0793$			
α	0.4735	0.4735	0.6559
β	0.68×10^{-4}	0.68×10^{-4}	0.20×10^{-3}
P Torr	200.0	247.3	327.9
T °K	280.6	303.5	299.6

TABLE II-1 Continued

	Initial Conditions State 1	After Normal Shock State 2	Final Equilibrium State 4
U m/sec	321.8	281.3	212.5
$[NO_2]$ moles/liter	0.827×10^{-3}	0.946×10^{-3}	0.173×10^{-2}
Exp 498 $M_s = 1.10$	$X_o = 0.0794$		
α	0.4790	0.4790	0.6730
β	0.68×10^{-4}	0.68×10^{-4}	0.22×10^{-3}
P Torr	200.0	255.2	337.3
T °K	281.0	307.5	301.3
U m/sec	326.5	279.9	210.6
$[NO_2]$ moles/liter	0.837×10^{-3}	0.976×10^{-3}	0.1821×10^{-2}
Exp 497 $M_s = 1.12$	$X_o = 0.0794$		
α	0.4790	0.4790	0.6860
β	0.68×10^{-4}	0.68×10^{-4}	0.24×10^{-3}
P Torr	200.0	264.8	348.3
T °K	281.0	311.7	302.8
U m/sec	331.6	278.0	208.5
$[NO_2]$ moles/liter	0.837×10^{-3}	0.998×10^{-3}	0.191×10^{-2}

TABLE II-1 Concluded

	Initial Conditions State 1	After Normal Shock State 2	Final Equilibrium State 4
Exp 494 M_s = 1.19 X_o = 0.0794			
α	0.4790	0.4790	0.7288
β	0.68×10^{-4}	0.68×10^{-4}	0.31×10^{-3}
P Torr	200.2	296.1	385.2
T °K	281.0	325.4	307.7
U m/sec	348.3	272.2	201.9
$[NO_2]$ moles/liter	0.837×10^{-3}	0.107×10^{-2}	0.220×10^{-2}
Exp 496 M_s = 1.21 X_o = 0.0794			
α	0.4790	0.4790	0.7487
β	0.68×10^{-4}	0.68×10^{-4}	0.35×10^{-3}
P Torr	200.2	311.5	403.3
T °K	281.0	331.8	310.2
U m/sec	356.1	270.0	199.0
$[NO_2]$ moles/liter	0.837×10^{-3}	0.110×10^{-2}	0.234×10^{-2}

TABLE II-2

	Initial Conditions State 1	After Normal Shock State 2	After Alpha Relaxation Beta Frozen	State 3	Final Equilibrium State 4
Exp 577	$M_s = 3.55$	$X_o = 0.0812$			
α	0.8448	0.8448	1.000	1.000	1.000
β	0.32×10^{-3}	0.32×10^{-3}	0.32×10^{-3}	0.162	0.962
P Torr	60.30	945.0	945.0	986.0	1035
T °K	294.7	1322	1305	1276	994.6
U m/sec	1104	316.1	315.8	302.4	235.6
$[NO_2]$ moles/liter	0.421×10^{-3}	0.147×10^{-2}	0.174×10^{-2}	0.154×10^{-2}	0.881×10^{-4}
Exp 581	$M_s = 3.91$	$X_o = 0.0812$			
α	0.8589	0.8589	1.000	1.000	1.000
β	0.35×10^{-3}	0.35×10^{-3}	0.35×10^{-3}	0.141	0.989
P Torr	57.00	1088	1087	1104	1164
T °K	295.6	1546	1533	1476	1225
U m/sec	1218	333.5	334.9	321.0	268.3
$[NO_2]$ moles/liter	0.403×10^{-3}	0.147×10^{-2}	0.171×10^{-2}	0.153×10^{-2}	0.241×10^{-4}
Exp 575	$M_s = 4.07$	$X_o = 0.0812$			
α	0.8646	0.8646	1.000	1.000	1.000

TABLE II-2 Continued

	Initial Conditions State 1	After Normal Shock State 2	After Alpha Beta Frozen	Relaxation State 3	Final Equilibrium State 4
β	0.35×10^{-3}	0.35×10^{-3}	0.35×10^{-3}	0.126	0.993
P Torr	49.00	1040	1038	1076	1102
T °K	294.6	1650	1639	1588	1336
U m/sec	1269	341.1	343.1	332.4	283.0
$[NO_2]$ moles/liter	0.356×10^{-3}	0.132×10^{-2}	0.152×10^{-2}	0.139×10^{-2}	0.128×10^{-4}
Exp 566	$M_s = 4.23$	$X_o = 0.0799$			
α	0.8846	0.8846	1.000	1.000	1.000
β	0.37×10^{-3}	0.37×10^{-3}	0.37×10^{-3}	0.116	0.996
P Torr	40.00	898	896.3	1457	943.6
T °K	294.2	1755	1748	1699	1454
U m/sec	1318	350.1	352.3	341.8	299.0
$[NO_2]$ moles/liter	0.288×10^{-3}	0.108×10^{-2}	0.122×10^{-2}	0.111×10^{-2}	0.601×10^{-5}
Exp 567	$M_s = 4.44$	$X_o = 0.0799$			
α	0.8971	0.8971	1.000	1.000	1.000
β	0.40×10^{-3}	0.40×10^{-3}	0.40×10^{-3}	0.103	0.997
P Torr	35.00	869.5	867.4	875.0	904.0
T °K	294.3	1906	1901	1855	1617

TABLE II-2 Continued

	Initial Conditions State 1	After Normal Shock State 2	After Alpha Relaxation Beta Frozen	After Alpha Relaxation State 3	Final Equilibrium State 4
U m/sec	1385	361.0	363.7	354.6	318.8
$[NO_2]$ moles/liter	0.255×10^{-3}	0.978×10^{-3}	0.108×10^{-2}	0.995×10^{-3}	0.315×10^{-5}
Exp 587	$M_s = 4.03$	$X_o = 0.0431$			
α	0.9163	0.9163	1.000	1.000	1.000
β	0.44×10^{-3}	0.44×10^{-3}	0.44×10^{-3}	0.0841	0.997
P Torr	50.20	1020	1018	1024	1054
T °K	294.6	1687	1683	1663	1516
U m/sec	1274	359.3	360.0	355.1	326.2
$[NO_2]$ moles/liter	0.208×10^{-3}	0.736×10^{-3}	0.802×10^{-3}	0.745×10^{-3}	0.247×10^{-5}
Exp 590	$M_s = 4.13$	$X_o = 0.0431$			
α	0.9307	0.9307	1.000	1.000	1.000
β	0.48×10^{-3}	0.48×10^{-3}	0.48×10^{-3}	0.0698	0.998
P Torr	40.30	856.1	856.2	860.0	883.5
T °K	294.6	1753	1750.5	1734	1586
U m/sec	1304	365.0	365.7	361.7	334.3
$[NO_2]$ moles/liter	0.169×10^{-3}	0.604×10^{-3}	0.648×10^{-3}	0.610×10^{-3}	0.148×10^{-5}

TABLE II-2 Concluded

	Initial Conditions State 1	After Normal Shock State 2	After Alpha Relaxation Beta Frozen	After Alpha Relaxation State 3	Final Equilibrium State 4
Exp 596	$M_s = 4.31$	$X_o = 0.0431$			
α	0.9435	0.9435	1.000	1.000	1.000
β	0.54×10^{-3}	0.54×10^{-3}	0.54×10^{-3}	0.0570	0.999
P Torr	34.90	810.0	809.8	812.0	830.8
T °K	295.7	1893	1891	1877	1731
U m/sec	1364	376.1	376.9	373.8	350.2
$[NO_2]$ moles/liter	0.148×10^{-3}	0.536×10^{-3}	0.567×10^{-3}	0.540×10^{-3}	0.859×10^{-6}
Exp 599	$M_s = 4.44$	$X_o = 0.0431$			
α	0.9522	0.9522	1.000	1.000	1.000
β	0.58×10^{-3}	0.58×10^{-3}	0.58×10^{-3}	0.0483	0.999
P Torr	29.00	716.0	716.4	717.1	783.2
T °K	295.7	1993	1991	1979	1802
U m/sec	1406	383.8	384.6	382.0	351.1
$[NO_2]$ moles/liter	0.124×10^{-3}	0.454×10^{-3}	0.476×10^{-3}	0.456×10^{-3}	0.529×10^{-6}

REFERENCES

1. Stupochenko, Ye. V., Losev, S. A., & Osipov, A. I. 1967 Relaxation in Shock Waves. New York: Springer-Verlag.

2. Wegener, P. P. 1959 Supersonic Nozzle Flow with a Reacting Gas Mixture. Phys. Fluids 2, 264.

3. Carrington, T. & Davidson, N. 1953 Shock Waves in Chemical Kinetics: The Rate of Dissociation of N_2O_4. J. Phys. Chem. 57, 418.

4. Wegener, P. P. 1958 Measurement of rate constants of fast reactions in a supersonic nozzle. J. Chem. Phys. 28, 724.

5. Cher, M. 1962 Rate of Dissociation of N_2O_4 by Ultrasonic Absorption Measurements. J. Chem. Phys. 37, 2564.

6. Bodenstein, M., Böes, H., Lindner, F. & Ramstetter, H. 1922 Bildung und Zersetzung des höheren Stickoxyde. Z. Physik Chem., 100, 68.

7. Rosser, W. A. & Wise, H. 1956 Thermal Decomposition of Nitrogen Dioxide. J. Chem. Phys. 24, 493.

8. Huffman, R. E. & Davidson, N. 1959 Shock Waves in Chemical Kinetics: The Thermal Decomposition of NO_2. J. Amer. Chem. Soc. 81, 2311.

9. Ashmore, P. G. & Burnett, M. G. 1962 Concurrent Molecular and Free Radical Mechanisms in the Thermal Decomposition of Nitrogen Dioxide. Faraday Soc. Trans. 58, 253.

10. Wegener, P. P. and Buzyna, G. 1969 Experiments on Shock Stand-Off Distance in Non-equilibrium Flow. J. Fluid Mech. 37, 325.

11. Einstein, A. 1920 Schallgeschwindigheit in teilweise dissoziierten Gasen. Sitzungsberichte d. preussischen Adak. d. Wiss. Wien, 18, 380.

12. Vincenti, W. G. & Kruger, C. H. Jr. 1965 Introduction to Physical Gas Dynamics. John Wiley & Sons.

13. Broer, L. J. F. 1950 On the influence of acoustic relaxation on compressible flow. Appl. Sci. Res. A, 2, 447.

14. Becker, E. & Böhme, G. 1969 Steady One-Dimensional Flow, Structure of Compression Waves. Gas Dynamics, a Series of Monographs, Vol. 1, Part I, pp. 71-117, Editor P. P. Wegener, Marcel Dekker, Inc., New York.

15. Wegener, P. P. & Cole, J. D. 1962 Experiments on propagation of weak disturbances in stationary supersonic nozzle flow of chemically reacting gas mixtures. Eighth Symposium (International) on Combustion. Baltimore: Williams and Wilkins Co.

16. Bethe, H. & Teller, E. 1941 Deviations from thermal equilibrium in shock waves. Cornell University unpublished report.

17. Griffith, W. C. & Kenny, A. 1957 On fully dispersed shock waves in carbon dioxide. J. Fluid Mech. 3, 286.

18. Lighthill, M. J. 1956 Viscosity Effects in Sound Waves of Finite Amplitude. Surveys in Mechanics, eds. G. K. Batchelor and R. M. Davis. Cambridge University Press, Cambridge.

19. Giauque, W. F. & Kemp, J. D. 1938 The entropies of nitrogen tetroxide and nitrogen dioxide. The heat capacity from 15 °K to the boiling point. The heat of vaporization and vapor pressure. The equilibria $N_2O_4 = 2NO_2 = 2NO + O_2$. J. Chem. Phys. 6, 40.

20. Strehlow, R. A. 1964 Private communication.

21. Gray, P. & Yoffe, A. D. 1955 The reactivity and structure of nitrogen dioxide. Chem. Rev. 55, 1069.

22. Fan, S. S. T. & Mason, D. M. 1962 Properties of the System $N_2O_4 \rightleftarrows 2NO_2 \rightleftarrows 2NO + O_2$. J. Chem. & Eng. Data 7, 183.

23. Svehla, R. A. & Brokaw, R. S. 1966 Thermodynamic and transport properties for the $N_2O_4 \rightleftarrows 2NO_2 \rightleftarrows 2NO + O_2$ system. NASA Technical Note, NASA TN D-3327.

24. U. S. Joint Army-Navy-Air Force Thermochemical Panel (JANAF) 1961 U. S. Air Force #AF33(616)-6149. Dow Chemical Company.

25. Gaydon, A. G. & Hurle, I. R. 1963 The Shock Tube in High-Temperature Chemical Physics. Chapman & Hall LTD London.

26. Spence, D. A. 1961 Unsteady shock propagation in a relaxing gas. Proc. Roy. Soc. 264, 221.

27. Liepmann, H. & Roshko, A. 1960 Elements of Gasdynamics. New York: John Wiley & Sons.

28. Hamming, R. W. 1959 Stable Predictor-Corrector Methods for Ordinary Differential Equations. J. ACM, 6, 37.

29. Peskin, J. R. & Rabinowitz, I. N. 1962 Diftran I and II. 650 Package Subroutines for the Solution of Systems of First Order Ordinary Differential Equations. Tech. Memo 154, Plasma Physics Lab., Princeton University, Princeton, N. J.

30. Hall, T. C. Jr. & Blacet, F. T. 1952 Separation of the absorption spectra of NO_2 and N_2O_4 in the range of 2400 - 5000 Å. J. Chem. Phys. 20, 1745.

31. Schott, G. & Davidson, N. 1958 Shock Waves in Chemical Kinetics: The Decomposition of N_2O_5 at High Temperatures. J. Amer. Chem. Soc. 80, 1841.

32. Zeldovich, Ya. B. & Raiser, Yu. P. 1966 Physics of Shock Waves and High-Temperature Hydrodynamic Phenomena. Vol. I New York: Academic Press.

33. Bauer, S. H. & Gustavson, M. R. 1954 Relaxation techniques for fast reactions: A study of the dissociation of Nitrogen Tetroxide. Discussions Faraday Soc. 17, 69.

34. Sessler, G. 1960 Schallausbreitung in teilweise Dissoziiertem gasförmigem Distickstofftetroxyd. Acustica 10, 44.

35. Frost, A. A. & Pearson, R. G. 1963 Kinetics and mechanisms; a study of homogeneous chemical reactions. New York: Wiley.

36. Eberstein, I. J. 1966 Shock Waves with Chemical Reactions in Shock Tubes. Yale University preprint for Report #4 Contract Nonr-609(46).

37. Eberstein, I. J. 1966 Evaluation of Light Deflection Technique for Detection of Transient Shock Waves. Rev. of Sci. Inst. 37, 959.

DOCUMENT CONTROL DATA - R & D

(Security classification of title, body of abstract and indexing annotation must be entered when the overall report is classified)

1 ORIGINATING ACTIVITY *(Corporate author)*
Yale University
New Haven, Conn. 06520

2a. REPORT SECURITY CLASSIFICATION
UNCLASSIFIED

2b. GROUP
N/A

3. REPORT TITLE
NON-EQUILIBRIUM FLOW FIELDS WITH CHEMICAL REACTIONS IN A SHOCK TUBE

4. DESCRIPTIVE NOTES *(Type of report and inclusive dates)*
Final Report June 1967 to June 1969

5 AUTHOR(S) *(First name, middle initial, last name)*
Elihu Zimet and Peter P. Wegener, Yale University

6. REPORT DATE
October 1969

7a. TOTAL NO. OF PAGES
75

7b. NO. OF REFS
37

8a. CONTRACT OR GRANT NO.
AF 40(600)-1133

b. PROJECT NO.
8952

c. Program Element 62201F

d. Task 08

9a. ORIGINATOR'S REPORT NUMBER(S)
AEDC-TR-69-229

9b. OTHER REPORT NO(S) *(Any other numbers that may be assigned this report)*
N/A

10 DISTRIBUTION STATEMENT
This document has been approved for public release and sale; its distribution is unlimited.

11 SUPPLEMENTARY NOTES
Available in DDC.

12. SPONSORING MILITARY ACTIVITY
Arnold Engineering Development Center, Air Force Systems Command, Arnold AF Station, Tenn. 37389

13 ABSTRACT
The present work is concerned with a theoretical and an experimental treatment of non-equilibrium flow of a chemically reacting gas mixture through a shock wave. The two chemical reactions given by $N_2O_4 + M = 2NO_2 + M = 2NO + O_2 + M$, where M represents the inert carrier gases argon or nitrogen, were studied. The experiments were carried out in a temperature controlled shock tube and a light absorption technique permitted the time dependent concentration of the species NO_2 to be determined. For shock strengths where the temperature did not exceed 400°K only the first chemical reaction took place. Stronger shock waves excited both chemical reactions with temperatures up to 2100°K, and for this reason, flow fields with two non-equilibrium modes could be investigated. Since the relaxation times of these two reactions were different by about three orders of magnitude, they could be experimentally uncoupled. A study of the reaction mechanisms and rate constants for both reactions was carried out. In general, the experimental work agreed well with an analytical description of the non-equilibrium flow fields, and with the work of previous investigators at conditions where direct comparisons could be made. At shock strengths exciting only the first chemical reaction the complete picture of a non-equilibrium flow field with only one non-equilibrium mode could be investigated. In this situation, the shock strengths were varied from weak, fully dispersed waves to strong, partly dispersed waves.

DD FORM 1 NOV 65 1473

14. KEY WORDS	LINK A		LINK B		LINK C	
	ROLE	WT	ROLE	WT	ROLE	WT
nonequilibrium flow						
shock tubes						
chemical reactions						
argon						
nitrogen						
shock waves						

AFSC
Arnold AFS Tenn